LBL-9554
UC-37

Lawrence Berkeley Laboratory
UNIVERSITY OF CALIFORNIA

DOSIMETRY, INSTRUMENTATION AND EXPOSURE CHAMBERS FOR DC MAGNETIC FIELD STUDIES

Tom S. Tenforde

March 1979

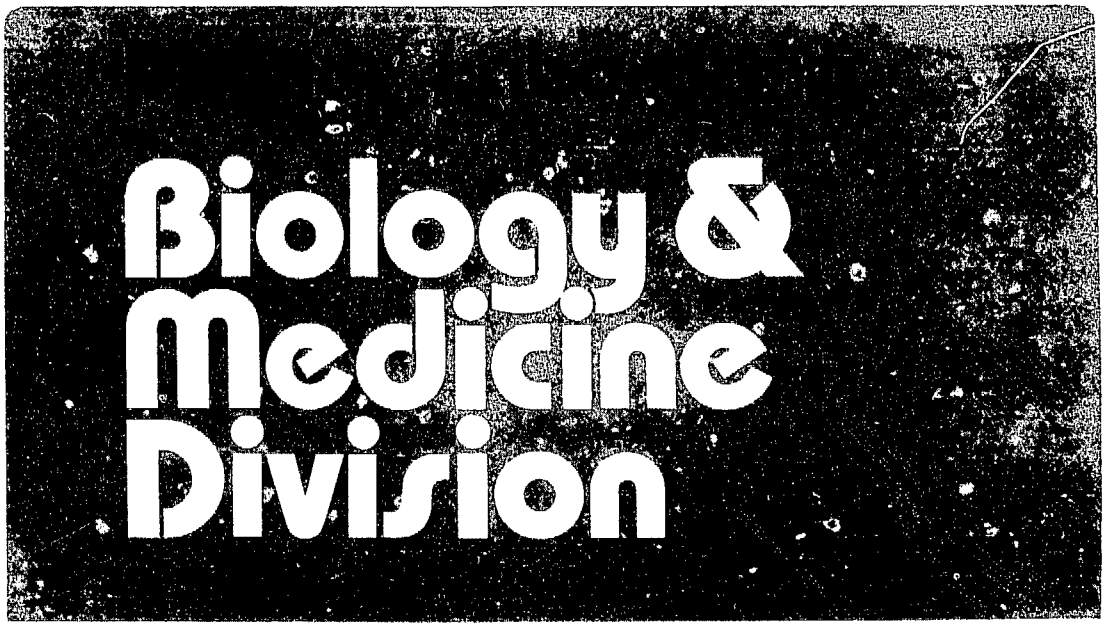

Prepared for the U.S. Department of Energy under Contract W-7405-ENG-48

LBL-9554

DOSIMETRY, INSTRUMENTATION AND EXPOSURE CHAMBERS FOR DC MAGNETIC FIELD STUDIES

Tom S. Tenforde

March, 1979

Biology & Medicine Division

Lawrence Berkeley Laboratory

University of California

Berkeley, California 94720

DOSIMETRY, INSTRUMENTATION AND EXPOSURE CHAMBERS FOR DC MAGNETIC FIELD STUDIES*

Tom S. Tenforde

Lawrence Berkeley Laboratory

The principal objective of this report is to describe in detail an exposure chamber that was developed at the Lawrence Berkeley Laboratory for automated, noninvasive studies of rodent physiology during exposure to high DC magnetic fields. A second objective is to discuss some of the unique instrumentation problems that must be overcome in order to record bioelectric signals from laboratory animals in the presence of a magnetic field. Finally, a description will be given of the various dosimetry techniques that can be employed for quantitation of magnetic field strength.

PROGRAMS

As a point of orientation, it is worthwhile to describe briefly the magnetic field programs now in progress at the Lawrence Berkeley Laboratory. An overview of the three current DOE-supported programs is given in Table I. The largest single program is directed towards the analysis of magnetic field effects and interaction mechanisms in a variety of biological systems, with the primary emphasis being placed on characterizing physiological parameters in small mammals exposed to intense DC fields. The second program is a retrospective epidemiological study of the health records of individuals occupationally exposed to fringe magnetic fields associated with cyclotron and bubble chamber operations. The third program involves the development of a

---

* Based in part on a talk presented at the workshop on "Extremely-Low-Frequency Electromagnetic Field Measurements in Biological Systems" held in Albuquerque, New Mexico, March 20 - 21, 1978.

compact magnetic field personnel dosimeter with data acquisition capabilities. The remainder of this report deals specifically with the facilities, instrumentation, dosimetry techniques and exposure chambers developed and utilized in the first of these three programs.

FACILITIES

Figs. 1 - 5 shows the facilities that were constructed for magnetic field experimentation during 1977 and the first half of 1978. Fig. 1 is a scale drawing of the magnet facility and the associated laboratory for experiment preparation. There are a total of five electromagnets, two of which are large-volume magnets with regions of homogeneous field in excess of two cubic feet. These large, 30-ton electromagnets are separately housed in a 600 ft^2 enclosure partitioned into two rooms with independent control of lighting and temperature. Fig. 2 is a frontal view of the magnet facility, showing the enclosure for the two large electromagnets, the central control console and two of the three small-volume electromagnets. Fig. 3 is a view of the SCR power supply bank, which converts 500 kilowatts of 480-volt AC power to DC for the electromagnets. The magnets and power supply units are cooled by a 160 g.p.m. flow of recirculating, low-conductivity water. Fig. 4 shows the electromagnet and the environmentally-controlled enclosure that have been set up for retinal and neural electrophysiology studies. The magnet has a 10-inch gap, a horizontal field and a peak DC field strength of 18 kilogauss. Fig. 5 is a view of the electromagnet and enclosure used for studies of animal physiology in DC fields up to 17 kilogauss strength. This magnet has a 7.625-inch gap and a vertical field. Fig. 6 shows the console from which the magnets can be operated by remote control. One of the console features is a 100-channel data acquisition unit (Acurex Autodata Nine) that is directly linked to various

electronic transducers and environmental monitors in the two magnet enclosures. The Autodata Nine unit, shown in Fig. 7, allows continuous monitoring to be performed at time intervals that are preset by the investigator. The data acquisition unit is also serially linked to a Texas Instruments Inc. Silent 700 ASR terminal for transfer of the data onto magnetic tape for subsequent computer analysis.

DOSIMETRY

Quantitation of the magnetic induction is routinely carried out by means of search coils and Hall effect probes. Field measurements with search coils are carried out by changing the magnetic flux linking a coil through one of three procedures: (1) rotation of the coil through 180°; (b) translation of the coil through a field gradient; (c) time-variation of the magnetic field strength. The resulting integrated e.m.f. from the search coil is measured with an electronic integrator and voltmeter. A small search coil placed on a precision positioning device is used to map the magnetic induction as a function of the current applied to the electromagnet coils, and also as a function of position within the gap of the electromagnet. A representative set of search coil measurements is shown in Fig. 8. In practice, the field is measured for the entire range of applied current in order to generate a precise plot of magnetic induction vs coil current. This plot is then used as a basis for adjusting the field strength via regulation of the current applied to the magnet coils. The adjustment of the exciting current is carried out by a direct measurement that uses a 20 A/mV shunt and a precision digital voltmeter, as shown in Fig. 9. Once adjusted, the current remains extremely stable over periods of weeks, with the maximum drift being less than 0.05%.

Another aspect of field stability that merits brief mention is the extent of the AC ripple field. At the time that the large-volume electromagnets were installed, it was observed that a 3 gauss, 360 Hz ripple field was present when the DC field was 15 kilogauss (see Fig. 10). Although small, this AC field led

to audible noise as a result of oscillatory forces between the magnet coil windings. We therefore installed low-pass filters on the power supplies for both of the large-volume electromagnets. As shown in Fig. 10, these filters attenuated the ripple currents and associated AC field by a factor of 100. Both the audible and ultrasonic noise levels were markedly reduced as a consequence of filtering out the AC ripple field.

For routine field monitoring and for continuous on-line recording of the magnetic induction, a variety of Hall effect probes are used. These probes are constructed of semiconducting material in which the current, carried by the majority charge carrier, interacts with an applied magnetic field via the Lorentz force and thereby produces a transverse electric field. Fig. 11 presents the relevant equations relating the magnetic induction, B, to the Hall electric potential, V_H. Fig. 12 shows a portable Model 620 gaussmeter obtained from the F. W. Bell Company, along with a flexible transverse Hall effect probe and a rigid axial probe. The transverse probe senses lines of magnetic induction that are perpendicular to the face of the probe, while the cylindrical axial probe measures the magnetic induction along its axis. The choice of a transverse or an axial probe for measurement of magnetic induction depends upon the geometry of the volume within which one wishes to determine the field strength. Flexible probe are obviously of utility for field measurements in relatively inaccessible locations, for example, within various types of exposure chambers. One application of a flexible probe is shown in Fig. 13, where a transverse probe is mounted in the center of a rodent exposure chamber for continuous on-line recording of the field. The probe is protected by a cover provided by a triangular exercise bar (shown at the upper left in Fig. 11), so that the rodents cannot molest it. The flexible probe is connected via extension cables to the rack-mounted Bell Model 615 gaussmeter shown in Fig. 14, which serves as a dedicated field-monitoring device. With each of the large-volume electromagnets, a permanently mounted Model 615 gaussmeter is used for continuous recording of the

magnetic induction throughout the course of an experiment.

Finally, it should be mentioned that an NMR gaussmeter is used for absolute field calibration. In general, the DC field measurements obtained by search coils, Hall effect probes, and the NMR gaussmeter agree to within 1%.

INSTRUMENTATION

One of the most challenging aspects of biomagnetic research is the development of instrumentation techniques and electronic devices that are unaffected by an applied field. The most common problems involve magnetization of ferromagnetic materials and the induction of Faraday potentials, both of which can produce quantitatively inaccurate or totally spurious electrical signals from monitoring devices. Examples of these problems will now be given in the context of three types of electrical recording techniques that are being used to monitor the physiological response of small mammals to strong magnetic fields.

The first of these techniques involves the use of implantable telemetry transducers for the measurement of deep-body temperature and cardiac activity. The telemetry transducers emit radiofrequency signals that reflect either the body temperature or the electrocardiogram, and thereby provide continuous non-invasive monitoring of circadian variations in these parameters. Fig. 15 shows a temperature telemeter, which is small silicone-encapsulated pill that contains a battery-driven thermistor and an RLC resonant circuit. The interpulse interval of the RF output signal reflects the body temperature. Fig. 16 shows a representative experimental set-up, in which a mouse bearing a temperature telemetry pill is housed in a cage that is wrapped with a pickup antenna loop. The antenna is connected to a receiver-demodulator unit that converts the pulse-interval-modulated signal into an analog voltage output, which can be calibrated to give a one volt increment for each 1 °C body temperature increment. A calibration curve showing the analog output vs temperature characteristics for a typical pill is shown in Fig. 17. Note that over the range of

interest for rodent deep-body temperature, 35 - 39 °C, the response characteristics are linear. This linear response feature of the output signal is obviously desirable because of the resultant simplification in data analysis.

In attempting to establish telemetry systems for monitoring physiological functions in rodents exposed to strong DC magnetic fields, two major problems had to be overcome. First, a conventional temperature telemeter was found to be inoperative in a field exceeding approximately 100 gauss because the oscillator had a ferrite core. This problem was solved by using an air-core oscillator. Secondly, the battery used in a conventional telemeter is highly magnetic, resulting in a strong orientational effect of an applied magnetic field. This problem was also easily solved by the use of a Ray-O-Vac nonmagnetic battery. With these two modifications of the commercially available temperature telemeter from Konigsberg Instruments Co., it was possible to successfully operate in fields as high as 20 kilogauss. Deep-body temperature profiles measured by telemetry for a mouse exposed to a 15.5 kilogauss field are shown in Figs. 18 and 19. The circadian variation in body temperature is clearly demonstrated by this set of data. Also, no obvious difference exists in daily body temperature profiles during the magnetic field exposure as compared with the pre-exposure and the post-exposure intervals.

A second instrumentation technique that poses special problems is the recording of action potentials from nerve tissue. As an example of such electrophysiological measurements, Fig. 20 demonstrates evoked action potentials recorded from frog sciatic nerves under control conditions and during exposure to a 20 kilogauss field. It is obvious from these oscillograms that the field has no effect on the action potential amplitude. In order to successfully carry out experiments of this nature in a strong magnetic field, two precautions must

be taken. First, nonmagnetic recording electrodes and leads must be used. Second, the oscilloscope must be shielded and/or placed at a sufficient distance from the magnet that the field does not distort the trace on the CRT.

A third type of electrical recording technique that can be used in a strong DC magnetic field under special conditions is electrocardiography. With this technique, it is important to avoid ferromagnetic material in the electrodes or the leads. The use of platinum electrodes has proved to be quite satisfactory for recording in fields as high as 20 kilogauss. Fig. 21 shows the electrocardiogram records for a rat exposed to magnetic fields up to 20.2 kilogauss strength. A marked augmentation of the T-wave signal is observed for fields in excess of 3 kilogauss, and the quantitative dependence of this phenomenon on field strength is shown in Fig. 22. A more detailed description of these observations has been given in a previous report (C. T. Gaffey and T. S. Tenforde, "Changes in the electrocardiograms of rats and dogs exposed to DC magnetic fields." Lawrence Berkeley Laboratory Report No. 9085; March 1979).

EXPOSURE CHAMBERS

As an introduction to this subject, it is worthwhile to briefly demonstrate by an example the types of artifacts that one can generate in magnetic field experiments when the environmental exposure conditions are poorly controlled. The series of experiments that will be used for illustration involved a measurement of activity patterns in Swiss mice after exposure to a 15.5 kilogauss field for a three-day period. Both the mice subjected to the magnetic field and the control mice were housed in conventional plastic cages with water bottles and pellet food. At the end of the exposure period, each individual mouse was taken from its cage and placed in one corner of a 30.5 cm x 30.5 cm x

15.5 cm chamber that was crossed by two photoelectric beams at right angles, thus dividing the enclosure into quadrants. As a mouse migrates from one quadrant to the next, the photocell and counting circuit record the event. In these activity experiments, the number of quadrant crossings was counted for each minute during a 5-min period. As shown in Fig. 23, panel (a), there was an apparent decrease in ambulatory activity of the mice exposed to the 15.5 kilogauss magnetic field. This experiment was repeated, and qualitatively similar results were obtained as shown in Fig. 23, panel (b). The third experiment was identical to the first two, except that the magnetic field was not turned on. The results of this experiment, shown in Fig. 23, panel (c), clearly demonstrated a reduced activity in the sham-exposed group relative to the control group. The results of the first two magnetic field experiments were therefore artifacts, which we believe to have occurred because the ambient light level in the magnet gap was only 5 ft-candles, as compared with 35 ft-candles in the open room where the cages for the control mice were kept. Other environmental factors, such as the ambient temperature and humidity, were similar for the controls and the experimental mice. It is therefore likely that the subdued light in the magnet gap was responsible for the reduced activity level of the experimental group.

In an effort to circumvent this type of artifactual result, a mouse exposure chamber has been designed that incorporates a number of environmental control features: (1) The temperature and humidity are closely regulated by supplying air that has been pre-conditioned in a plenum, with the temperature control being accomplished through a feedback circuit that utilizes a thermistor sensor located in the mouse cage. (2) The lighting is controlled to 15 ± 2 ft-candles by an overhead light pipe assembly. (3) The mouse population

is provided ample space, approximately 10 in^2 per mouse, to prevent stress associated with overcrowding. (4) All sources of audible and ultrasonic noise resulting from oscillatory forces induced by the magnetic field are eliminated or attenuated to a level less than 10 dB above the ambient field-off level.

Fig. 24 presents a schematic diagram of the mouse exposure chamber containing the above environmental controls, and Fig. 25 is a photograph of the chamber without the overhead light pipe. The chamber occupies the central 2 ft x 2 ft region of homogeneous field within the gap of the 17 kilogauss electromagnet shown in Fig. 5. In addition to providing a well-controlled environment during exposure to the field, the aluminum cage and its lucite support frame contain a number of transducers that permit the noninvasive monitoring of several physiological functions. These automated measurements include the continuous recording of body weight, respiration and climbing activity. A 2 ft x 2 ft lucite cage frame wrapped with a copper loop antenna can be used in place of the aluminum cage for telemetry measurements of deep-body temperature and cardiac activity. In addition, the exposure chamber provides mechanisms for the convenient recording of food intake and urine and feces excretion. These various physiological measurements, as well as the environmental controls and the monitoring systems for temperature, humidity and magnetic field strength, will next be described in detail.

LIGHT CONTROL

A rigorous control of lighting is of importance in experiments with rodents for two reasons: (1) the uniformity of lighting throughout the exposure chamber will affect the ambulatory behavior of rodents, insofar as they exhibit a preference for regions of the cage with the lowest light intensity; (2) the dominant factor in the phasing of circadian rhythms in activity and physiological variables is the light/dark cycle.

Achieving uniform light intensity over a 4 ft^2 area within a strong magnetic field proved to be a difficult, although not insurmountable, problem. Because of a magnetic field effect on fluorescent light beams, the source of light must be incandescent lamps. In order to avoid stress on the filaments, it was decided to place the lamps outside of the magnet gap and to distribute the light within the cage by means of a light pipe, shown in Fig. 26. The light pipe that was constructed at the Lawrence Berkeley Laboratory consists of a ½-inch-thick sheet of lucite that is 3.5 ft long and 2 ft wide. The 2 ft x 2 ft area over the mouse exposure chamber has been etched by sand-blasting in order to diffuse the light. The source of white light is an array of 15 GE bulbs, each with 18 Watts output, that are placed at the end of the light pipe protruding beyond the magnet gap. In order to focus the light over the 4 ft^2 sand-blasted surface, the remainder of the light pipe has been covered with a layer of silver foil. Our initial expectations that this design would provide uniform lighting throughout the exposure chamber proved to be incorrect, as shown in panel (a) at the left of Fig. 27. It is quite obvious from the photometer readings that the light intensity varies by a factor of more than five between the region of the light pipe that is proximal to the lamps and the distal region. This problem was initially very frustrating, but the solution ultimately proved to be very simple, namely, to construct a "countergradient filter". This was achieved by spraying India ink on a cellulose acetate substrate placed over the sand-blasted diffusing surface of the light pipe. By appropriate variation of the opacity of the filter, it was possible to achieve a remarkably uniform light level of 15 $\pm$ 2 ft-candles over the entire 4 ft^2 surface of the light pipe that covers the exposure chamber. The countergradient filter is shown in Fig. 28 and the light profile over the light pipe surface is shown in panel (b) on the right side of Fig. 27. It should also be noted that the array of fifteen 18-Watt bulbs that serve the

light pipe have a considerable thermal output, and are therefore cooled by a continuous flow of air supplied through the flexible hose shown in Fig. 26. The bulbs are protected by an over-temperature regulator which is part of the assembly that controls the light on / light off cycle. This control unit, shown in Fig. 29, also contains a timer with stops that can be set to regulate the light on / light off periods. In a routine operating mode, the timer is set to turn the lights on at 06:00 hours and off at 18:00 hrs. In the absence of an overriding applied stress, this regimen leads to circadian rhythms in activity and physiological parameters for rodents that peak in the middle of the dark cycle.

ENVIRONMENTAL TEMPERATURE AND HUMIDITY CONTROLS

The close regulation of ambient temperature and relative humidity within the exposure chamber is achieved by a forced draft of conditioned air pulled by a fan from the Wedco incubator shown in Fig. 30. The incubator is provided with both heating and cooling units, and the temperature in the exposure chamber is maintained within $\pm$ 0.5 °C of a preset value by means of a feedback regulation circuit. This regulator consists of a heating/cooling control mounted on the Wedco incubator, which responds to a thermistor probe inserted in the outlet port of the exposure chamber. The draft of conditioned air is passed through the chamber at a rate of five complete exchanges per hour. The environmental temperature is continuously recorded by copper-constantin thermocouples inserted in the inlet and outlet ports on the exposure chamber, and this information is recorded on the Autodata Nine data acquisition unit. Simultaneous recordings are made of the relative humidity based on readings by a Hygrocon probe placed in the outlet portal. This probe and the humidity recording unit are shown in Fig. 31.

STRAIN GAGE MONITORS FOR WEIGHT AND CLIMBING ACTIVITY

The floor of the exposure chamber is supported by four corner strain-gage transducers for continuous monitoring of the variation in body mass and the center of gravity coordinates of the rodent population. Similarly, the exercise bar shown in Fig. 13 is mounted on two strain-gage transducers for monitoring the activity of the rodent population as a function of time. These six transducers were custom made by NDT Consultants from nonmagnetic materials; close-up views of one of the corner transducers for the cage and one of the activity bar transducers are shown in Figs. 32 and 33, respectively. The strain gages resolve weight changes as small as one gram, and they have extremely linear output vs load characteristics, as shown in Fig. 34. The outputs in microvolts from the strain gages are continuously recorded on six channels of the Autodata Nine data acquisition unit. With appropriate scaling factors that relate the analog output in microvolts to the load in gm-weight, the sum of the recorded outputs from the four corner strain gages gives the total body mass, and the sum of the two activity bar strain gages gives the total weight applied to the bar. As shown in Fig. 35, the weights recorded on the four corner strain gages can be used to compute the center-of-mass coordinates of the rodent population at any instant of time.

It is worth remarking that the first approach that was taken to measure weight and activity involved the use of aneroid transducers rather than strain gages. These devices are small fluid-filled metal pill boxes that operate by producing a change in the fluid pressure in response to an applied force. The pressure change is then converted to an analog voltage output. This concept initially seemed reasonable, but when the first aneroid transducers were fabricated, it was found that the operating characteristics and temperature sensitivity of each aneroid unit were quite different. Consequently, for each

aneroid transducer it would have been necessary to introduce a different factor to convert the output voltage into an equivalent gm-weight, thereby complicating the data analysis. A similar problem does not exist for the strain-gage transducers, which can be adjusted to yield identical output vs load characteristics for different gages.

FEEDING ASSEMBLY

From several preliminary studies with a conventional metabolic cage, it was apparent that a major problem could arise from contamination of the urine and feces collector with the pellet food supplied from a hopper. Even if the hopper was separated from the floor of the cage by a corridor and the food pellets were finely pulverized, the rodents consistently pulled food into the cage and dropped it through the floor into the urine and feces trays. The resultant mixing of food and excreta is clearly undesirable since it would affect not only the weights of the urine and feces samples, but would also influence measurements of chemical parameters such as protein nitrogen in the urine specimens. In order to circumvent this problem, liquid diet supplied by the Grand Island Biological Company can be used to provide the nutritional and water requirements of the rodents. The use of liquid diet could conceivably lead to problems such as diarrhea and tooth overgrowth. However, in test experiments of several weeks duration, no evidence was obtained that either of these problems accompanied the use of liquid diet.

The liquid diet is supplied to the exposure chamber from a 250 ml bottle and six lines of PVC tubing, shown in Fig. 36. The tubing is terminated by spring-loaded nozzles that prevent dripping of the liquid. These nozzles, and the six brass guides that position them in the wall of the exposure chamber, are shown in Fig. 37. All of the components of the feeder assembly can be autoclaved to ensure antiseptic conditions at the initiation of an experiment. The bottle

that supplies the liquid diet is connected to the PVC tubing via a manifold and a "quick-disconnect" valve. During the course of an experiment, the bottle is removed approximately once a day for addition of new liquid diet, and is replaced by a freshly sterilized bottle at 2 - 3 day intervals. The consumption of liquid diet by the rodent population can be recorded using volumetric marks on the side of the supply bottle. If desired, the bottle can also be removed at the quick-disconnect valve and weighed on a top-loading balance.

EXCRETA COLLECTION

The initial approach that was taken to achieve the collection of urine and feces without cross-contamination involved the fabrication of the tray shown in Fig. 38. This tray, which can be easily inserted beneath the exposure chamber on guide rails, contains an array of bars that have a triangular vertex and a rounded lower surface. The shape of the bars was patterned after the pendulum-shaped urine collector used in a conventional metabolic cage. The object of this design is to collect urine in a trough at the base of each bar, while the fecal pellets are collected in troughs at the sides of the bar. The triangular vertex of the bar is intended to deflect the fecal pellets into these side troughs, while the urine is guided by the round lower surface of each bar into the collecting trough immediately below it. Preliminary tests quickly demonstrated that this excreta tray was unsatisfactory since the urine splashed into the feces collectors, and the fecal pellets frequently adhered to the triangular surfaces of the bars. It should be remarked that this problem was not totally unexpected, since similar observations had been made in pilot studies with a commercially available metabolic cage.

As an alternative approach, a simple tray insert was fabricated that consists of a lucite trough overlaid by a screen made from nonmagnetic stainless steel with a 0.05-inch mesh diameter. The trough, shown in Fig. 39, is V-shaped and the two

sides have a 7° downward slope that causes the urine to drain to the center, thereby facilitating collection with a syringe. The mesh of the stainless steel screen, shown in Fig. 40, is sufficiently small to allow collection of fecal pellets with 100% efficiency. Preliminary tests have demonstrated that the collecting tray does, in fact, give a complete separation of urine and feces. The one disadvantage of this design is the fact that the urine passes through the feces collecting screen, with an associated risk of bacterial and fungal contamination. This problem, however, can be circumvented by collecting the urine at frequent intervals and freezing the specimens in capped vials. If desired, small quantities of antibiotic and antifungal agents can be added to the urine samples.

CARBON DIOXIDE MEASUREMENTS

As an index of respiration by the rodents confined to the exposure chamber, the air passing through the chamber is continuously monitored for carbon dioxide content. After passing the outlet port of the chamber, the air is pulled through the dehumidifying unit shown in Fig. 41 by means of a small pump. The air then passes through an infrared monitor, shown in Fig. 42, for quantitation of the carbon dioxide concentration. The dehumidification is required in order to remove water vapor that interferes with the measurement of carbon dioxide based on infrared absorption. As shown by the calibration curve in Fig. 43, the infrared absorption is a linear function of carbon dioxide concentration up to 1%. In practice, the carbon dioxide content of air passing through the exposure chamber is less than 0.2%, and therefore falls within the linear response range of the analyzer.

The analog output of the infrared monitor is recorded on the Autodata Nine data acquisition unit, thereby permitting continuous monitoring of the carbon dioxide concentration. In preliminary tests with mice placed on a 12-hr light / 12-hr dark schedule, a peak carbon dioxide output was observed in the middle of

the dark period. This observation conforms to the expectation that the respiration of the rodent population should be a maximum at the time of their maximum activity.

* * * * * *

In conclusion, the numerous problems that confront the investigator attempting to devise exposure chambers for magnetic field experimentation may appear awesome, but with a sufficient investment of effort, satisfactory solutions to the problems generally emerge. The situation is reminiscent of an anecdote about Thomas Edison, who, in the midst of solving a particularly difficult technical problem, was confronted by the words of a frustrated assistant: "Mr. Edison, we have tried this experiment one hundred times, and we have failed one hundred times. Surely we should now give up!" Somewhat disdainfully, Edison replied to his assistant: "Failed? No, we haven't failed. On the contrary, we have succeeded in learning one hundred things that don't work!"

TABLE I. SUMMARY OF MAGNETIC FIELD BIOMEDICAL AND DOSIMETER DEVELOPMENT PROGRAMS AT THE LAWRENCE BERKELEY LABORATORY

MAGNETIC FIELDS - BIOMEDICAL EFFECTS

(Biology & Medicine Division Project 4407)

ANIMAL PHYSIOLOGY	RETINAL AND NEURAL ELECTROPHYSIOLOGY	DEVELOPMENTAL STUDIES	MOLECULAR STUDIES
T. Tenforde C. Gaffey L. Levy	M. Raybourn J. Dixon	T. Yang L. Craise	R. Roots

MAGNETIC FIELD EPIDEMIOLOGY	ENGINEERING AND INSTRUMENTATION	DOSIMETER DEVELOPMENT
(Project 4409) T. Budinger P. Wong C.-K. Yen	C. Dols D. Nelson	(Instrument Techniques Division Project 4965) F. Goulding T. Fujita A. Biocca M. Breen

FIGURE LEGENDS

Fig. 1. Scale drawing of the magnetic field research facility and the associated laboratory for experiment preparation. The two large-volume electromagnets, denoted Apollo and Amphion, are housed in a 600 ft^2 enclosure partitioned into two rooms with separate control of lighting and temperature. The facility also contains two small electromagnets, denoted Julius and Ceasar, and a set of Helmholtz coils (not shown). The SCR power supplies are served by 1600 amps of 480-volt, 3-phase power. The magnets and power supplies are cooled by recirculating low-conductivity water (denoted LCW in the drawing).

Fig. 2. Front view of the control console and the enclosure for the two large-volume electromagnets.

Fig. 3. The SCR power supplies are shown, along with the power boxes that provide an outlet for 500 kilowatts of 480-volt AC power.

Fig. 4. Front view of the Apollo electromagnet, which has a 10-inch gap and produces a horizontal DC field up to 18 kilogauss strength. The two racks contain instrumentation for electrophysiological studies on neural and retinal tissues.

Fig. 5. Side view of the Amphion electromagnet, which has a 7.625-inch gap and produces a vertical field up to 17 kilogauss strength. Instrumentation for automated physiology studies is shown in the background.

Fig. 6. Front view of the central control console, showing the Autodata 9 data acquisition unit and the Texas Instruments Silent 700 ASR terminal.

Fig. 7 Close-up view of the Autodata 9 and TI Silent 700 ASR units.

Fig. 8. Search coil measurements in the Amphion electromagnet, showing the magnetic induction as a function of applied current and position within the gap.

Fig. 9. Digital voltmeter recording of the 20 A/mV shunt potential used to set the current applied to the coils of the Amphion electromagnet.

Fig. 10. Oscillograms showing attenuation by a low-pass filter of the AC ripple current from the SCR serving the Amphion electromagnet.

Fig. 11. Relationship between the magnetic induction, B, and the Hall potential, V_H, for a transverse Hall effect sensor.

Fig. 12. Bell Model 620 portable gaussmeter, with a transverse flexible probe (nearest to gaussmeter) and a rigid axial probe (foreground).

Fig. 13. Flexible transverse probe mounted within a magnetic field exposure chamber for rodents. During experiments, the probe is covered by the triangular exercise bar shown in the background.

Fig. 14. Rack-mounted Bell Model 620 gaussmeter used for continuous on-line recording of the magnetic field strength in the large-volume electromagnets.

Fig. 15. Implantable, silicone-encapsulated telemetry pill for monitoring deep-body temperature. The pill consists of a battery-driven thermistor and an oscillator circuit that sends out pulse-interval-modulated radio-frequency signals.

Fig. 16. Set-up for telemetry recording of deep-body temperature in a mouse. The cage containing the subject is placed within a pick-up loop antenna that is connected to a receiver-demodulator unit shown in the background. The pulse-interval-modulated signal refecting the deep-body temperature is shown on the oscilloscope screen behind the mouse cage.

Fig. 17. Plot of the analog output from a receiver-demodulator unit showing a nearly linear voltage-temperature relationship over the range 35 - 40 °C.

Figs. 18 and 19. Deep-body temperature profiles for an LAF_1/J mouse during control conditions and during exposure to a 15.5 kilogauss field. Continuous records of the body temperature were made during a 5-day pre-exposure control interval, a 5-day exposure to the magnetic field, and a 5-day

post-exposure control interval. The mouse was maintained on a 12-hr light / 12-hr dark schedule throughout the 15-day period. Error bars in Fig. 18 represent one standard deviation of the temperature recorded at each time on 5 consecutive days. The records during each segment of the experiment show clear evidence for a circadian rhythm in body temperature, which peaks in the middle of the dark cycle. The total daily variation in temperature is approximately 2 °C. From the intercomparison of temperature records shown in Fig. 19, there appears to be no effect of exposure to the magnetic field on the circadian variation in deep-body temperature.

Fig. 20. Oscillograms showing evoked action potentials from frog sciatic nerves under control conditions and during a 30-min exposure to a 20 kilogauss field. The amplitude of the maximal action potential was unaffected by exposure to the field. (Courtesy of Dr. C. Gaffey, Biomedical Division, Lawrence Berkeley Laboratory).

Figs. 21 and 22. Electrocardiogram records are shown for a female Buffalo rat during control conditions and during exposure to a DC magnetic field ranging in strength up to 20.2 kilogauss. The field-strength-dependent augmentation of the T-wave amplitude, which is evident from the electrocardiogram records reproduced in Fig. 21, is plotted in Fig. 22.

Fig. 23. The activity of Swiss mice was measured after a 3-day exposure to a 15.5 kilogauss field, and compared with the activity of control mice. Activity was scored as the number of times per minute that each individual mouse moved from one quadrant to the next in a chamber that was divided into four sectors by two photoelectric beams. In each experiment, the control and exposed (or sham-exposed) groups each contained a total of 15 to 19 mice. Difference between the activity of the control and the exposed (or sham-exposed) groups were significant at

the level $p < 0.001$, $p = 0.059$ and $p = 0.064$ in the experiments shown in panels a, b and c, respectively.

Fig. 24. Schematic diagram of the exposure chamber for automated physiological studies on mice exposed to DC magnetic fields. The surface area of the floor of the cage is 4 ft^2, which fills the region of homogeneous field in the Amphion electromagnet. The maximum DC field strength that can be achieved by this magnet is 17 kilogauss.

Fig. 25. Photograph of the exposure chamber for magnetic field studies. The feeder assembly and the overhead light pipe are not attached.

Fig. 26. Light pipe for the exposure chamber shown in Fig. 25. The 4 ft^2 area that covers the cage has been sand-blasted to diffuse the light, which is supplied by an array of fifteen 18 Watt GE bulbs in the aluminum casing at the far end of the light pipe. The other surfaces of the light pipe have been covered with silver foil to focus the light towards the sand-blasted surface. The light bulbs are cooled by a continuous flow of air provided by the small fan shown in the background.

Fig. 27. Photometer readings are listed for different sections of the 4 ft^2 diffusing surface of the light pipe shown in Fig. 26. The light profile on the right side of the figure was obtained after addition of the countergradient filter shown in Fig. 28.

Fig. 28. Photograph of the countergradient filter that provides uniform lighting over the 4 ft^2 diffusing surface of the light pipe shown in Fig. 26. The filter was prepared by spraying India ink onto a cellulose acetate substrate. A photometer was used to judge the intensity and uniformity of the transmitted light, and the opacity of the filter was adjusted to give an illumination of 15 ± 2 ft-candles

over the entire surface (right-hand panel in Fig. 27). A photographic reproduction of the original India ink filter was prepared for use in the exposure chamber. The filter is protected by means of a 0.067-inch-thick lucite overlay.

Fig. 29. On / off timer and overtemperature regulator for the light source used on the light pipe assembly shown in Fig. 26.

Fig. 30. Photograph of the Wedco incubator used to regulate the temperature and humidity of the air supplied to the mouse exposure chamber. The air flow rate is regulated by the fan mounted on the right side of the incubator. A thermistor probe in the exposure chamber outlet port and a feedback circuit are used to maintain the temperature within $\pm$ 0.5 °C of a preset value.

Fig. 31. Photograph of the Hygrocon humidity sensor and recording unit. The probe contains a metallic strip with electrical resistance characteristics that are sensitive to the relative humidity. As shown in the foreground, the probe is placed in the path of air passing through the outlet portal on the exposure chamber.

Fig. 32. Photograph of the strain-gage transducer that supports one corner of the cage floor within the mouse exposure chamber.

Fig. 33. Photograph of the strain-gage transducer that supports one end of a triangular exercise bar for monitoring rodent activity patterns. A portion of the exercise bar is shown in the background.

Fig. 34. Microstrain vs load characteristics are plotted for one of the four corner strain gage transducers that support the cage floor, and for one of the two strain gages that support the exercise bar. The four corner strain gages are calibrated to give identical operating characteristics at the initiation of an experiment, and a similar procedure is followed for the two activity bar strain gages.

Fig. 35. Equations are presented that give the total body mass and the center-of-mass coordinates of the rodent population from the weights recorded on the four corner strain gages that support the cage floor.

Fig. 36. Photograph of the liquid diet feeder assembly. The reservoir is attached via a "quick-disconnect" valve to a manifold that supplies six feeder ports.

Fig. 37. Photograph of the spring-loaded nozzle on one liquid diet feeder; the six nozzles are inserted into the side of the exposure chamber by means of cylindrical brass guides.

Fig. 38. Photograph of the excreta collecting tray containing an array of bars with triangular vertices and rounded lower surfaces for the separation of urine and feces.

Fig. 39. Photograph of the urine collecting tray that is inserted under the cage floor on guide rails. The sides of the tray have a 7° downward slope to facilitate urine collection in the central trough.

Fig. 40. Photograph of the nonmagnetic stainless steel screen that is placed over the urine tray for collection of feces. The mesh diameter of 0.05 inch is sufficiently small to provide a 100% separation of urine and feces, without significant retention of urine on the surface of the screen.

Fig. 41. Dehumidifier unit that removes water vapor from the air passing through the outlet port of the mouse exposure chamber. The dehumidified air is then pulled by a small pump into an infrared analyzer for measurement of the carbon dioxide concentration.

Fig. 42. Photograph of the Lira infrared analyzer used to measure the carbon dioxide. The carbon dioxide content of air leaving the

mouse exposure chamber provides an index of the rate of respiration by the rodent population.

Fig. 43. Plot of the absorbance (in arbitrary units) measured by the Lira infrared analyzer as a function of carbon dioxide concentration. A linear response is observed for carbon dioxide concentrations up to 1%.

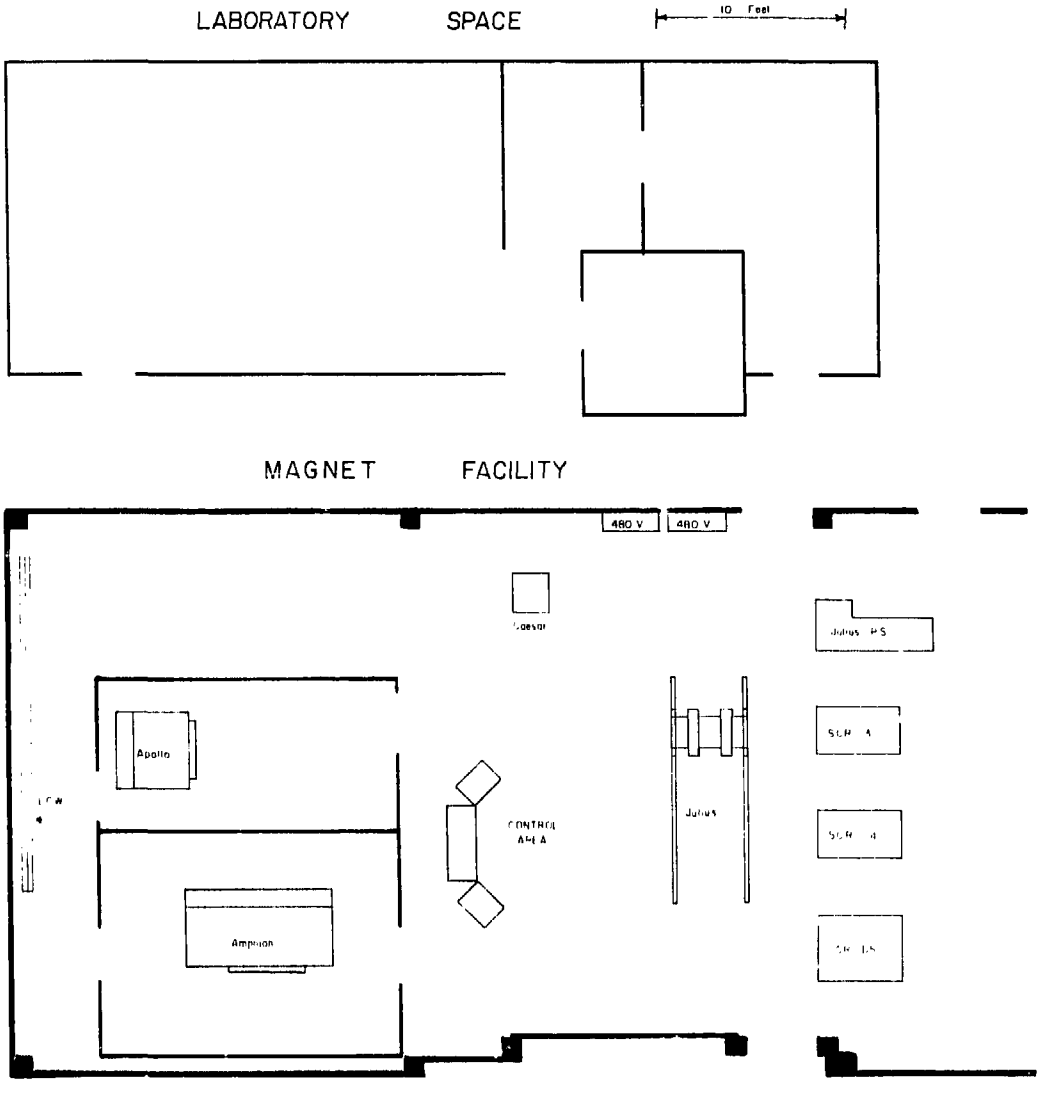
LABORATORY SPACE
10 Feet
MAGNET FACILITY
480 V
480 V
Caesar
Julius P.S.
Apollo
Julius
CONTROL AREA
Ampion
XBL 781-6922

FIGURE 1

CBB 780-13-35

FIGURE 2

CBB 784-4804

FIGURE 3

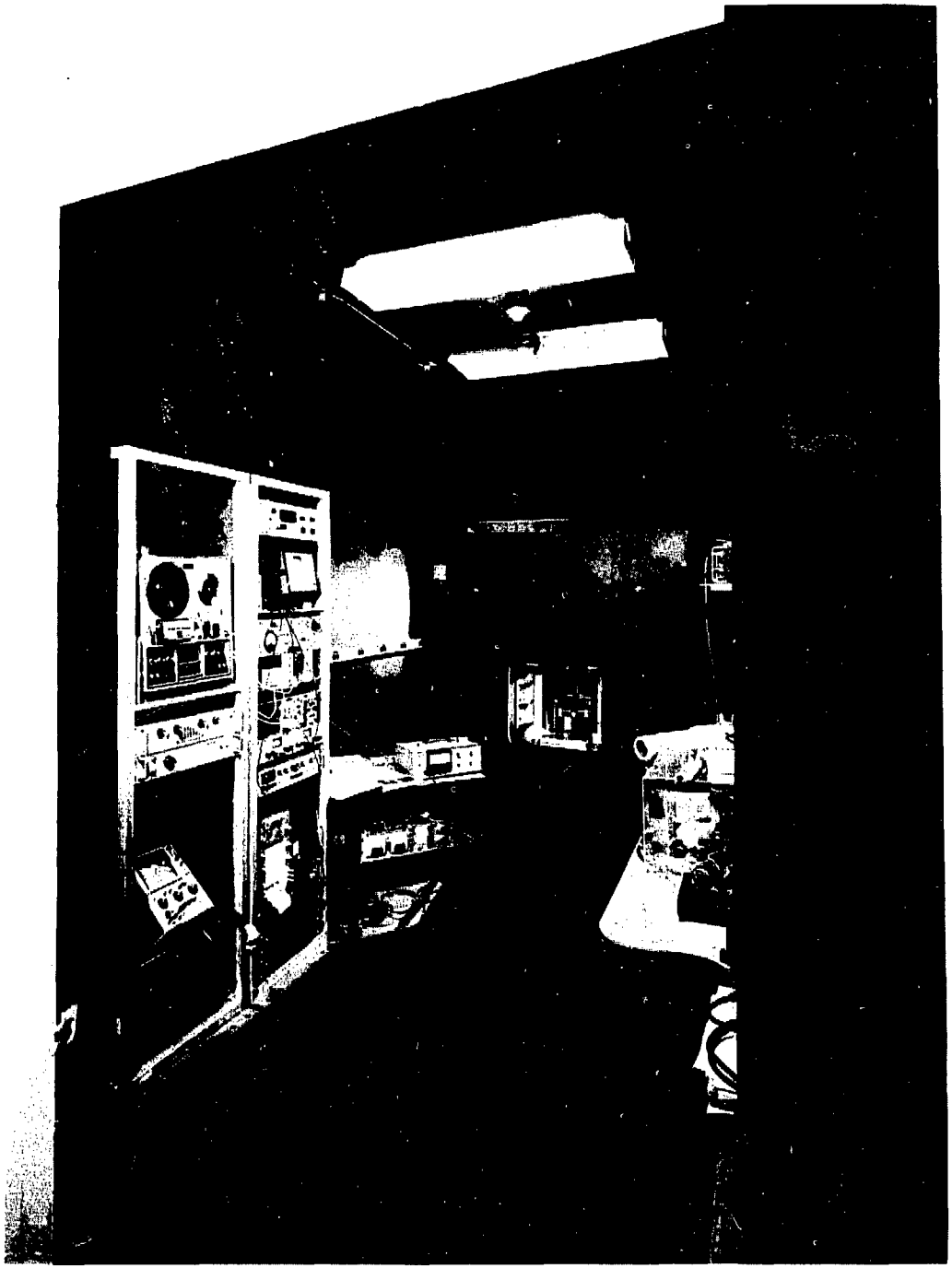

FIGURE 4 CBB 780-13037

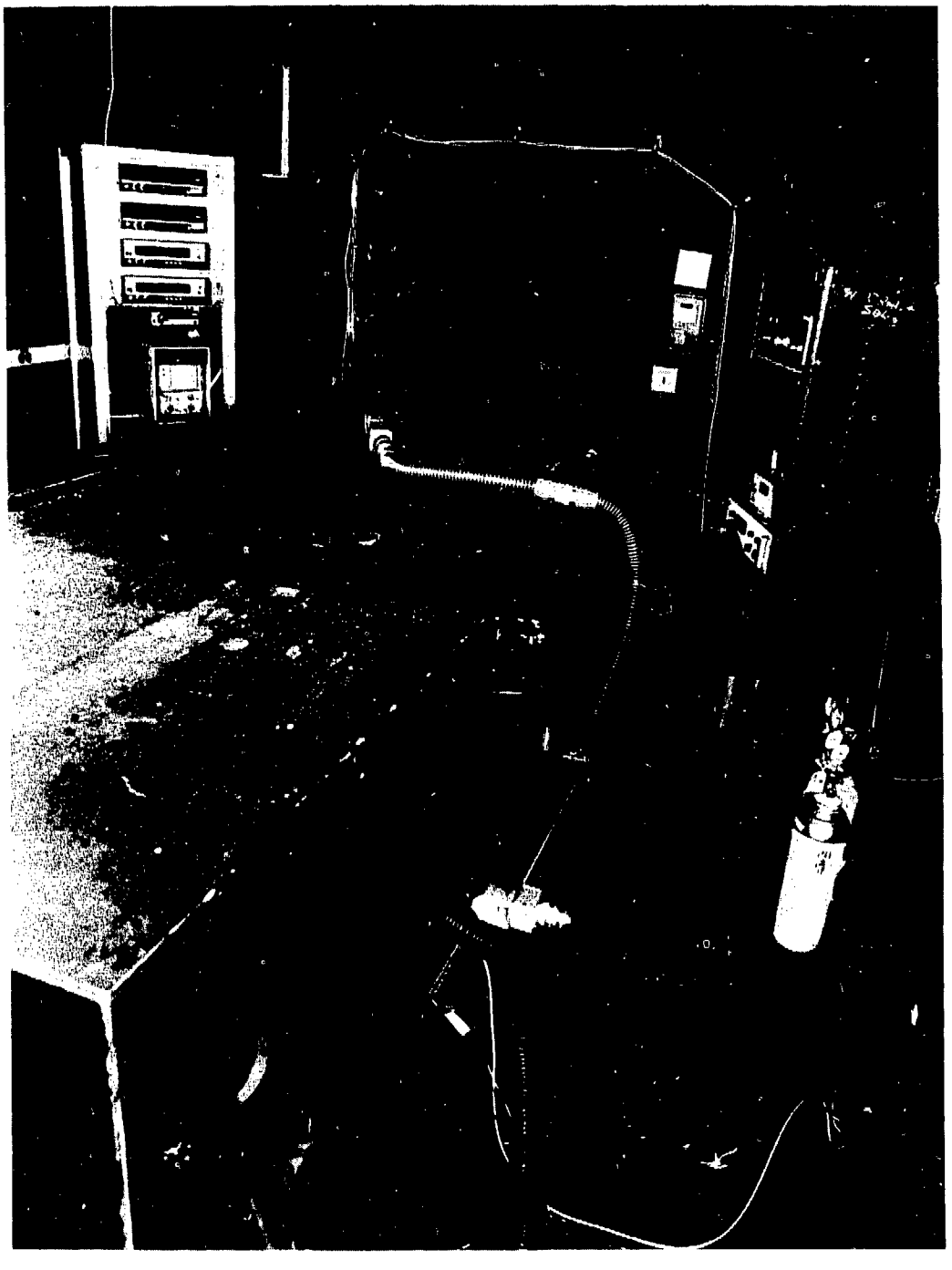

FIGURE 5 CBB 790-15730

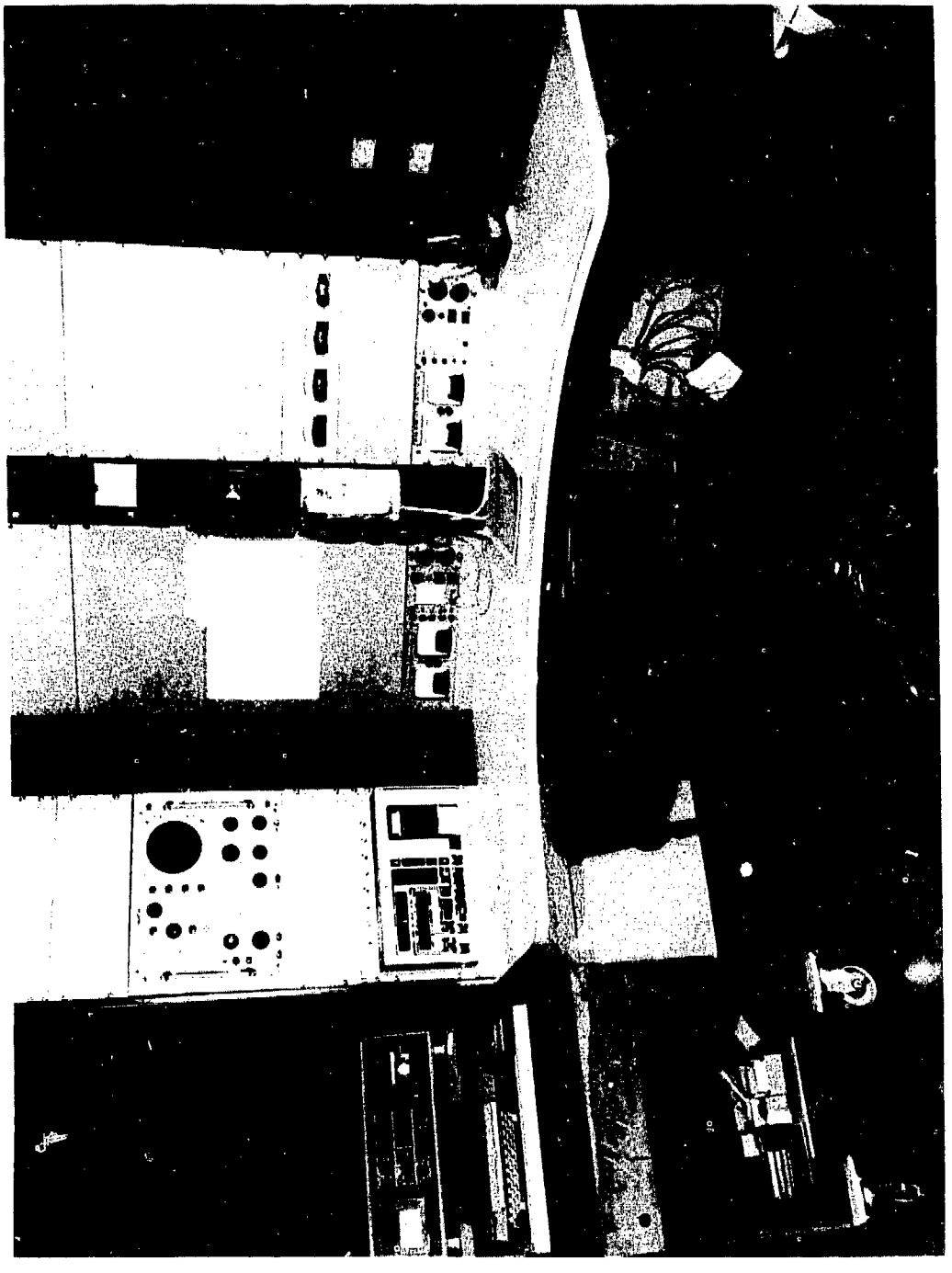

CBB 790-2422

FIGURE 6

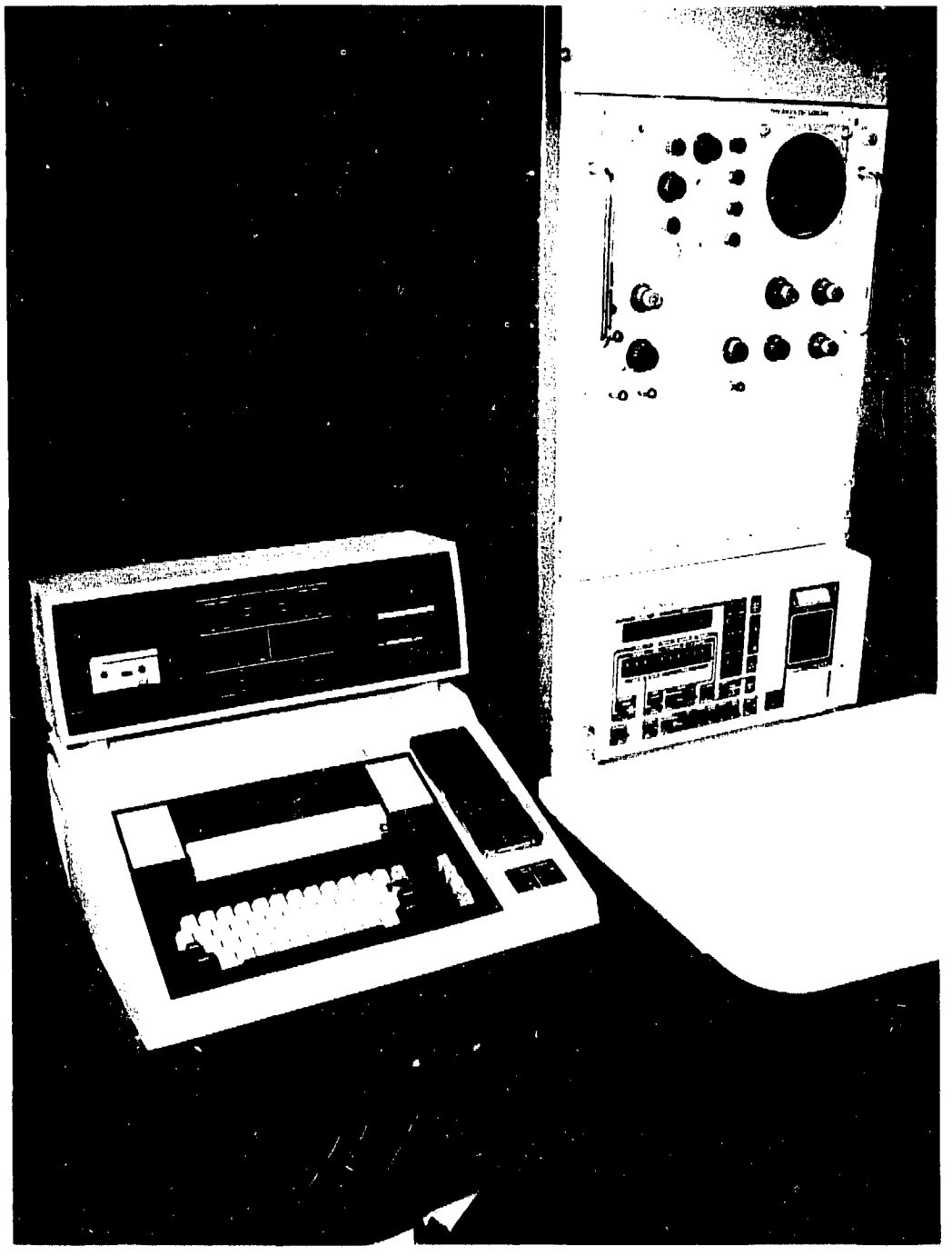

FIGURE 7 CBB 792-2384

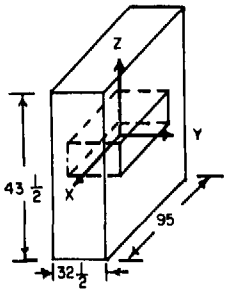

AMPHION MAGNETIC FIELD PROFILE

ALONG BEAM AXIS

(29" x 32" x 7 5/8")

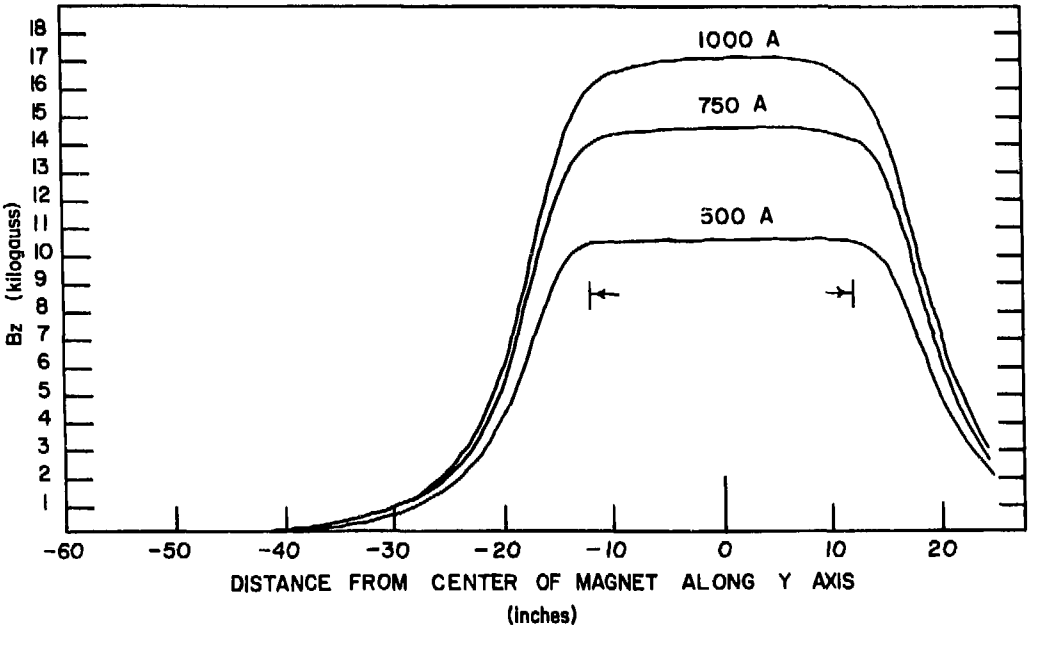

XBL 781-7068

FIGURE 8

CBB 790-2416

FIGURE 9


Unfiltered power supply input
Filtered power supply output
200V
2V
2msec

FIGURE 10

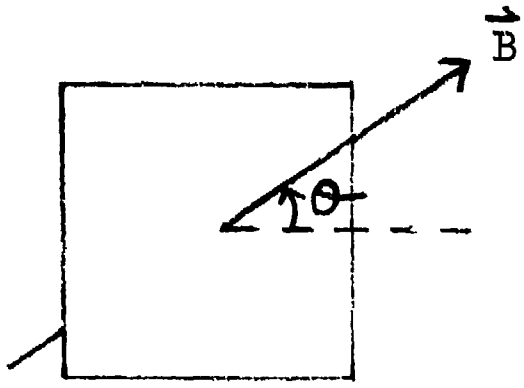

$$V_H = \gamma |B| \sin\theta$$

where γ = magnetic sensitivity in mV/kG at rated current

XBL 793-8792

FIGURE 11

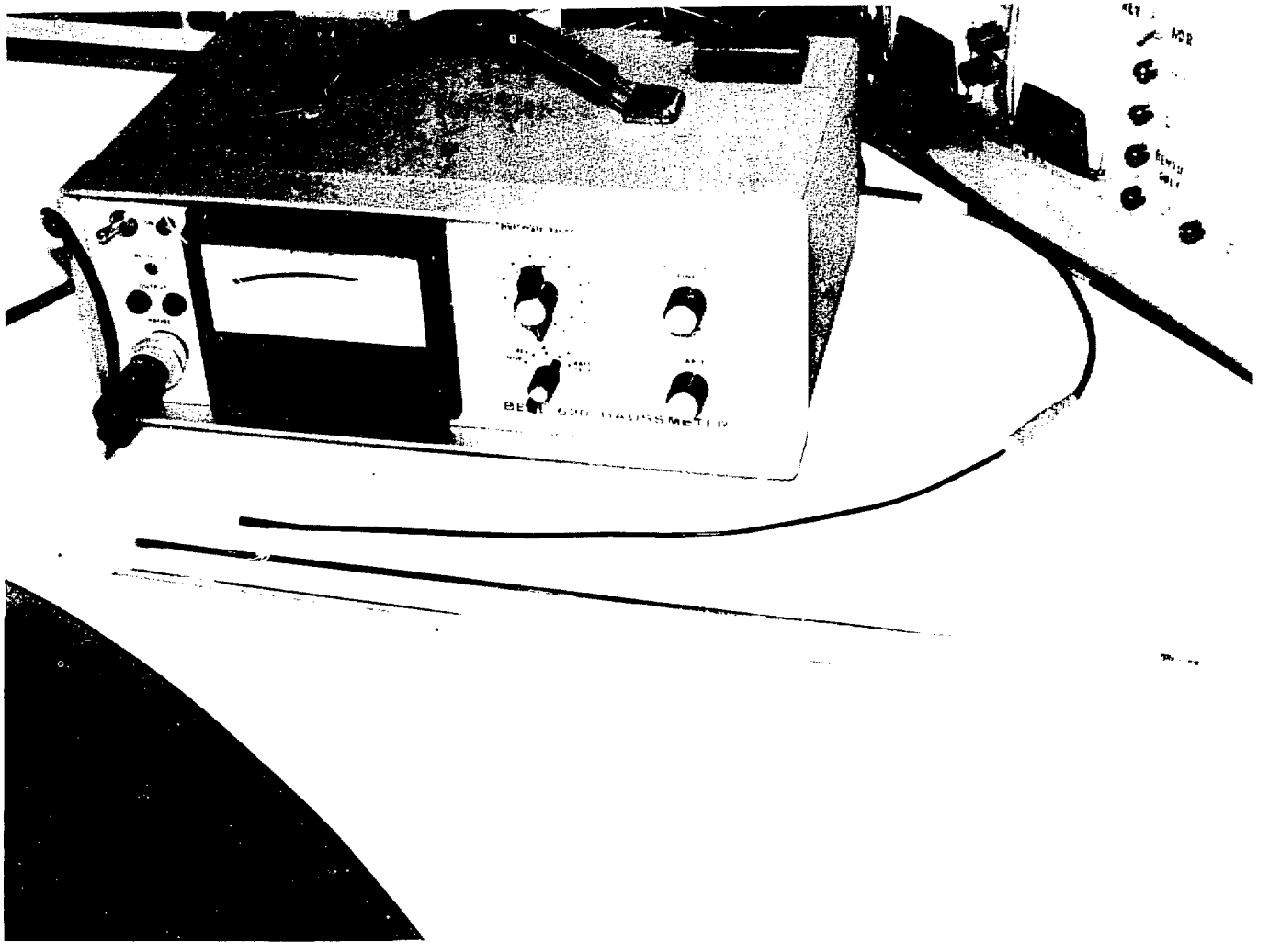

FIGURE 12

CBB 790-2711

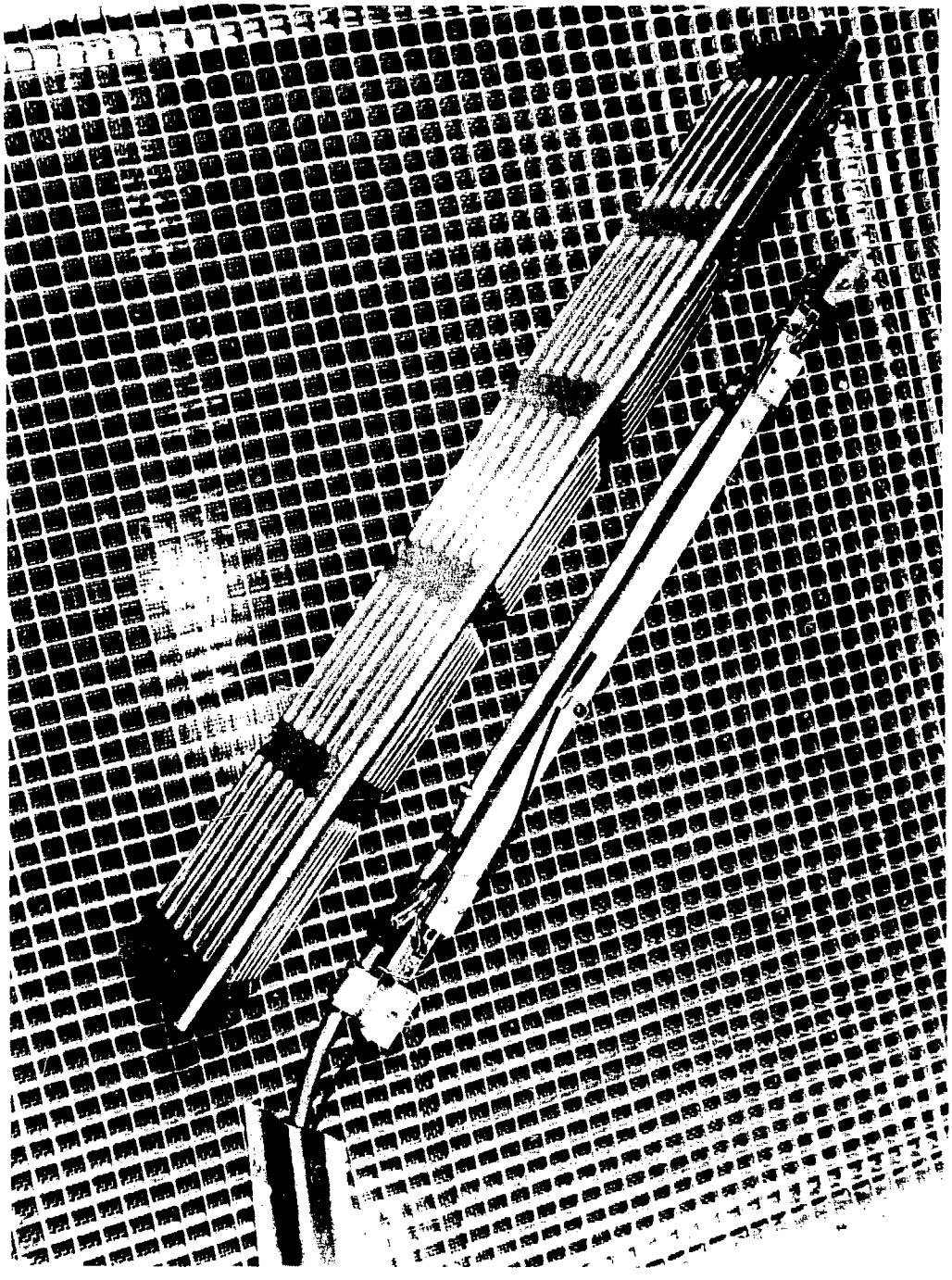

FIGURE 13 CBB 790-2408

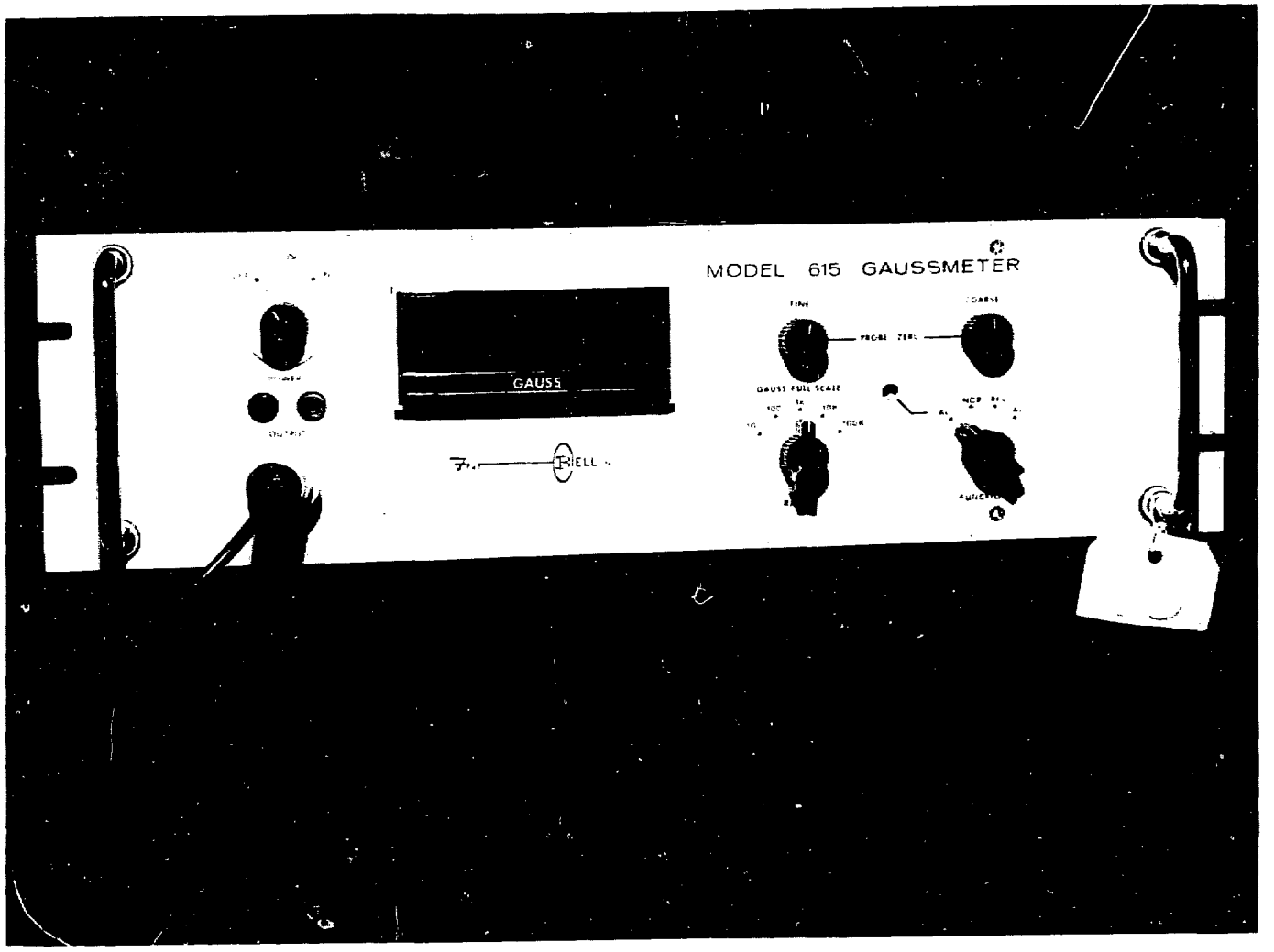

FIGURE 14

CBB 790-2420

FIGURE 15

XBB 783-3437

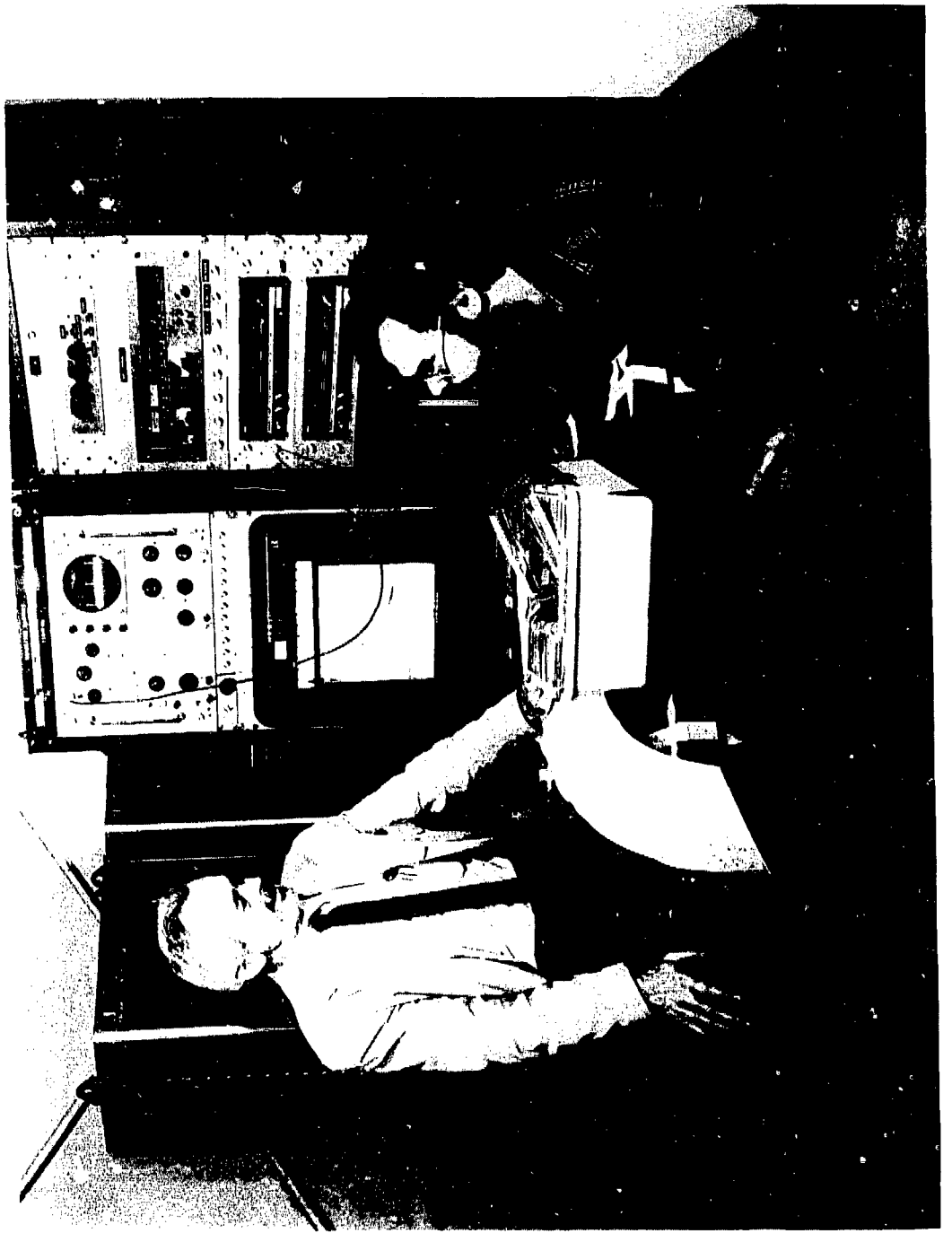

CBB 770-10484

FIGURE 16

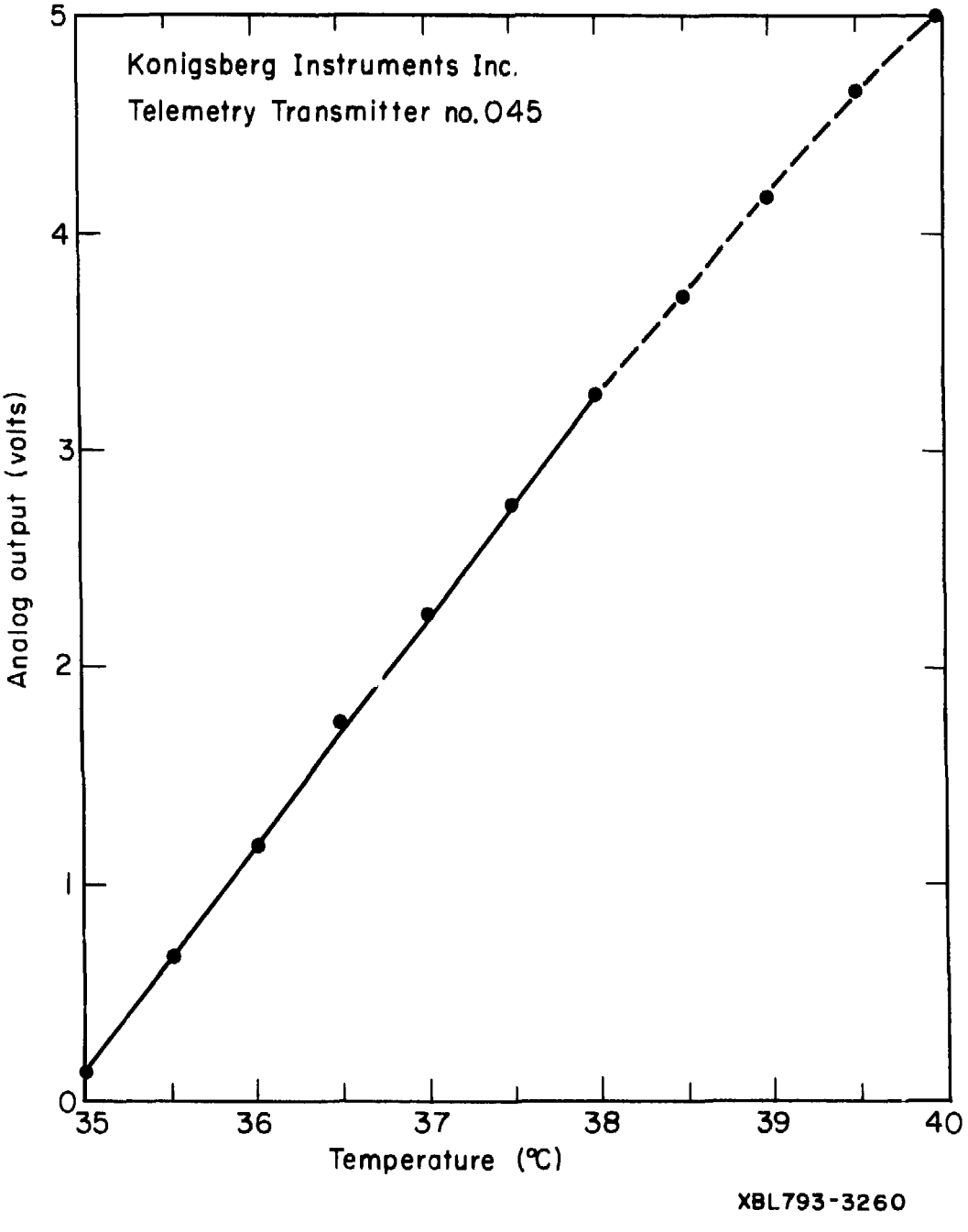
Konigsberg Instruments Inc.
Telemetry Transmitter no.045
Analog output (volts)
0
1
2
3
4
5
35
36
37
38
39
40
Temperature (°C)
XBL793-3260

FIGURE 17

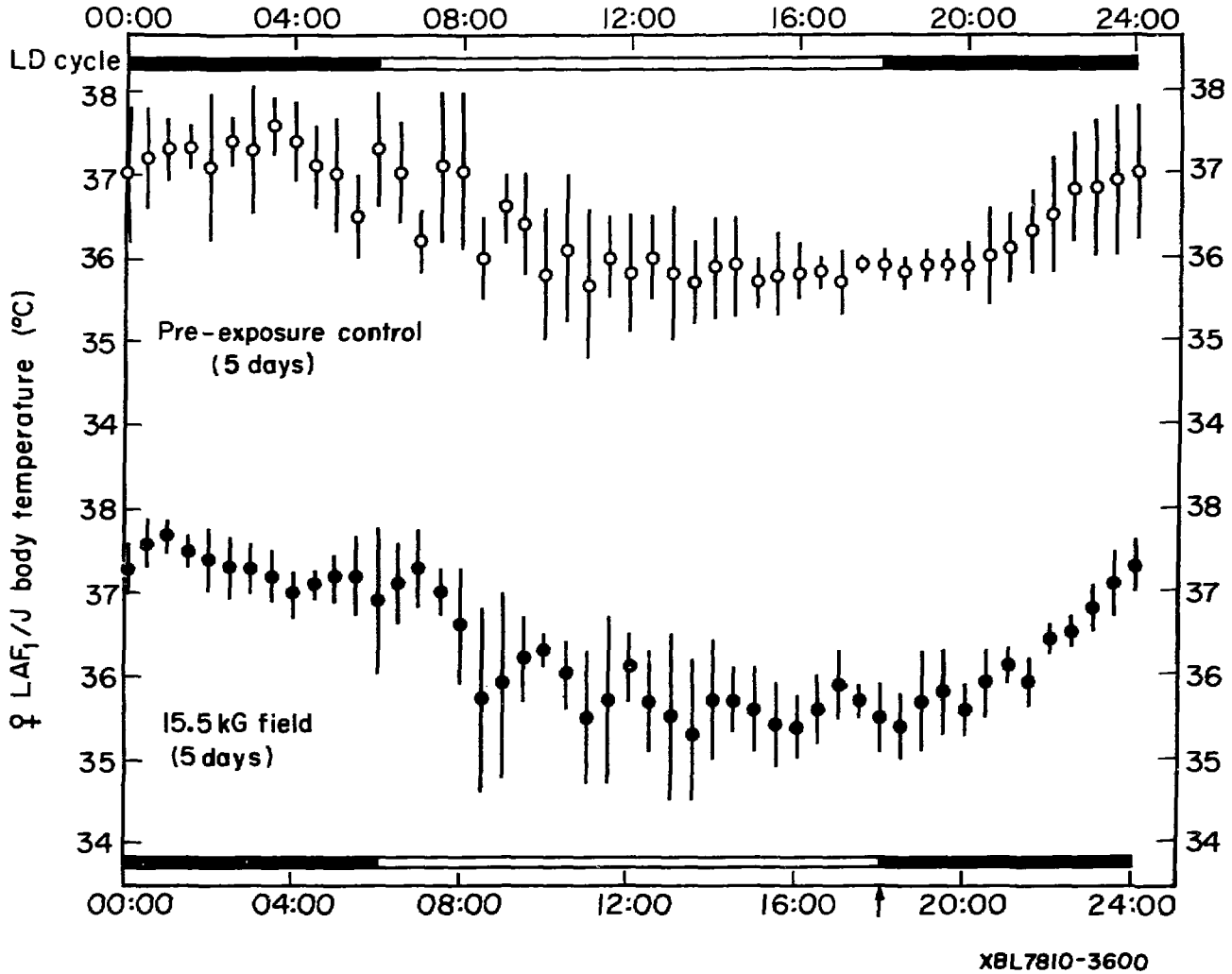
00:00
04:00
08:00
12:00
16:00
20:00
24:00
LD cycle
38
37
36
35
34
♀ LAF1/J body temperature (°C)
Pre-exposure control
(5 days)
15.5 kG field
(5 days)
XBL7810-3600

FIGURE 18

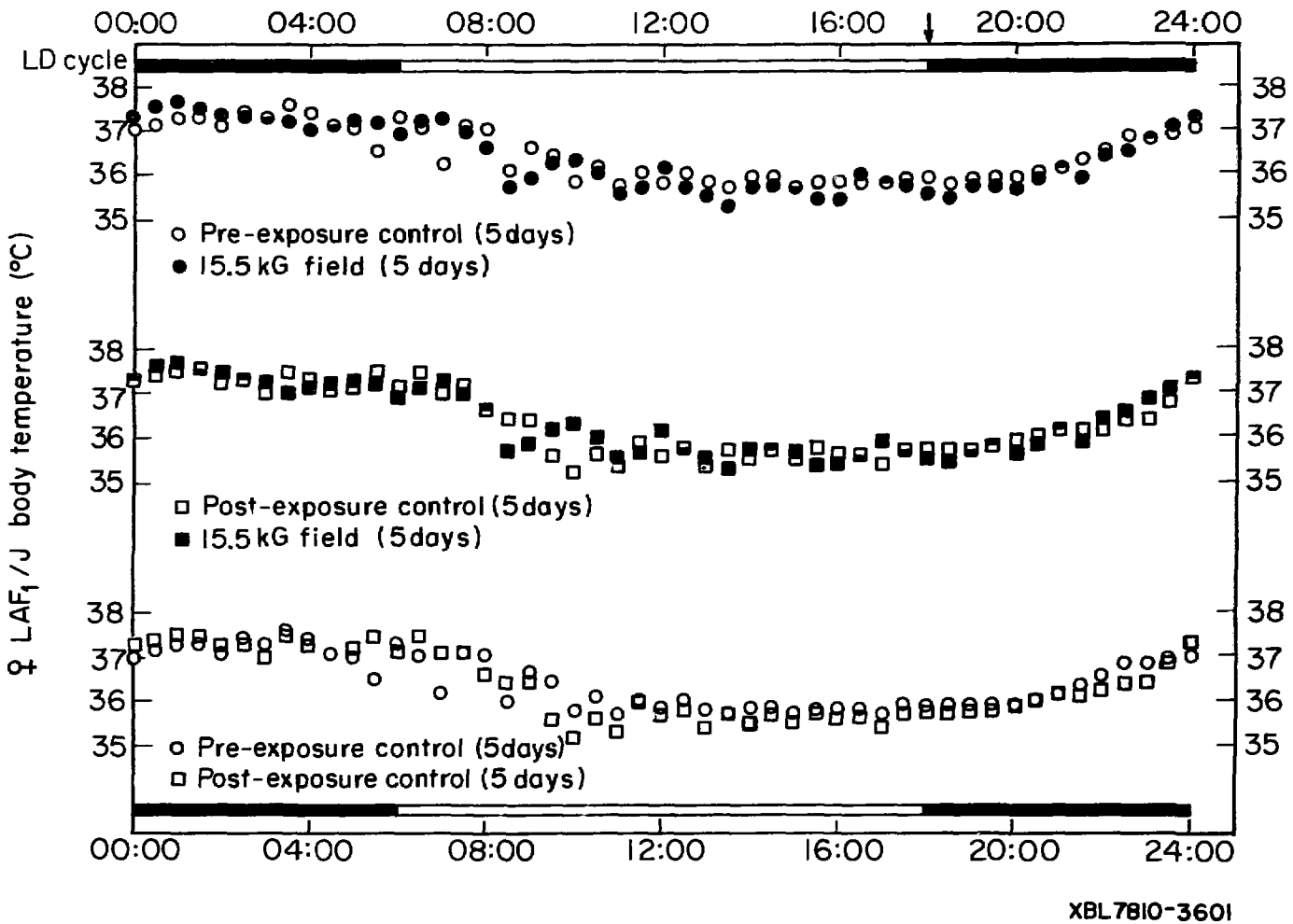
00:00
04:00
08:00
12:00
16:00
20:00
24:00
LD cycle
38
37
36
35
o Pre-exposure control (5days)
● 15.5 kG field (5 days)
□ Post-exposure control (5days)
■ 15.5 kG field (5days)
o Pre-exposure control (5days)
□ Post-exposure control (5 days)
♀ LAF1/J body temperature (°C)
XBL7810-3601

FIGURE 19

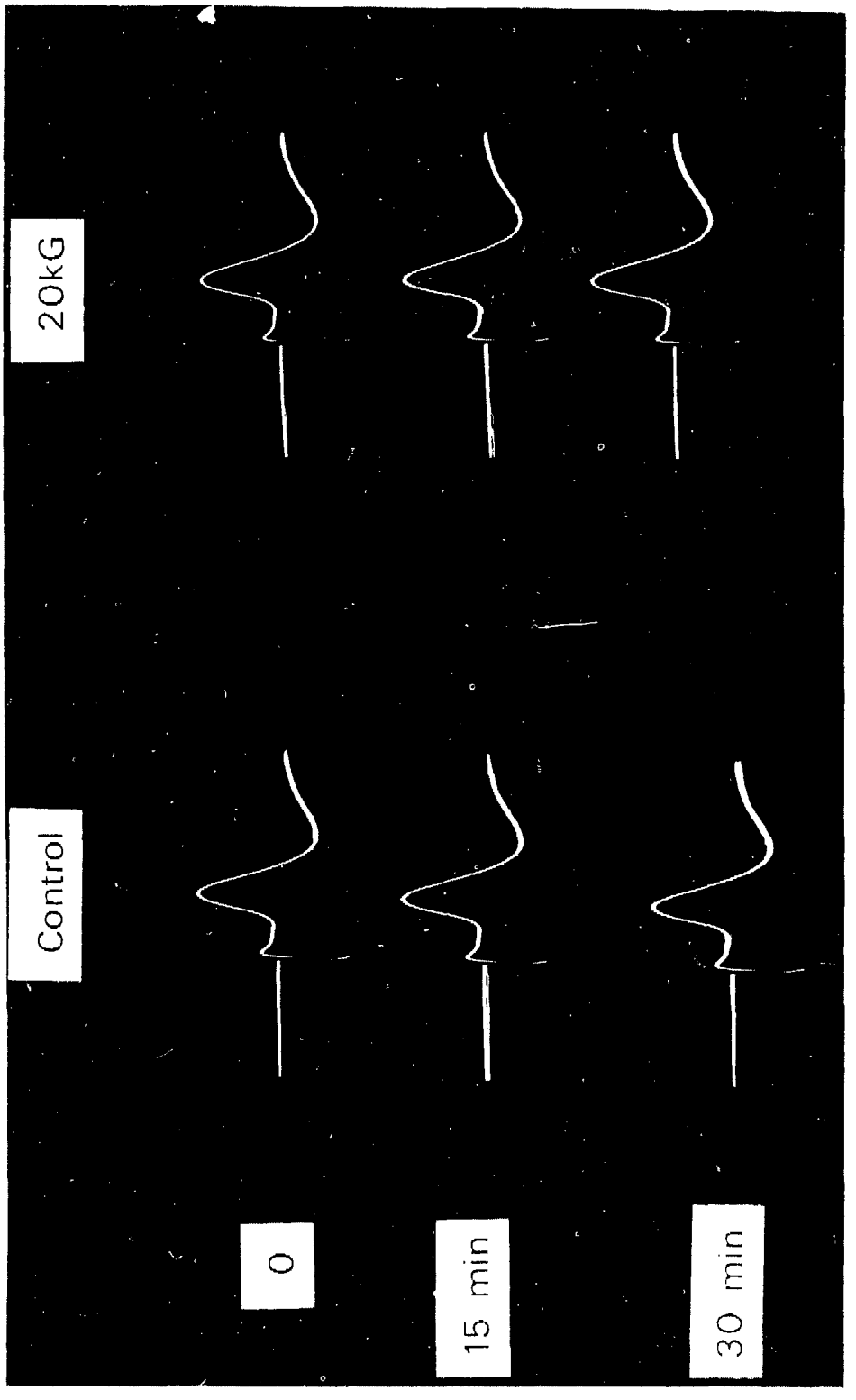

FIGURE 20

XBB 780-12959

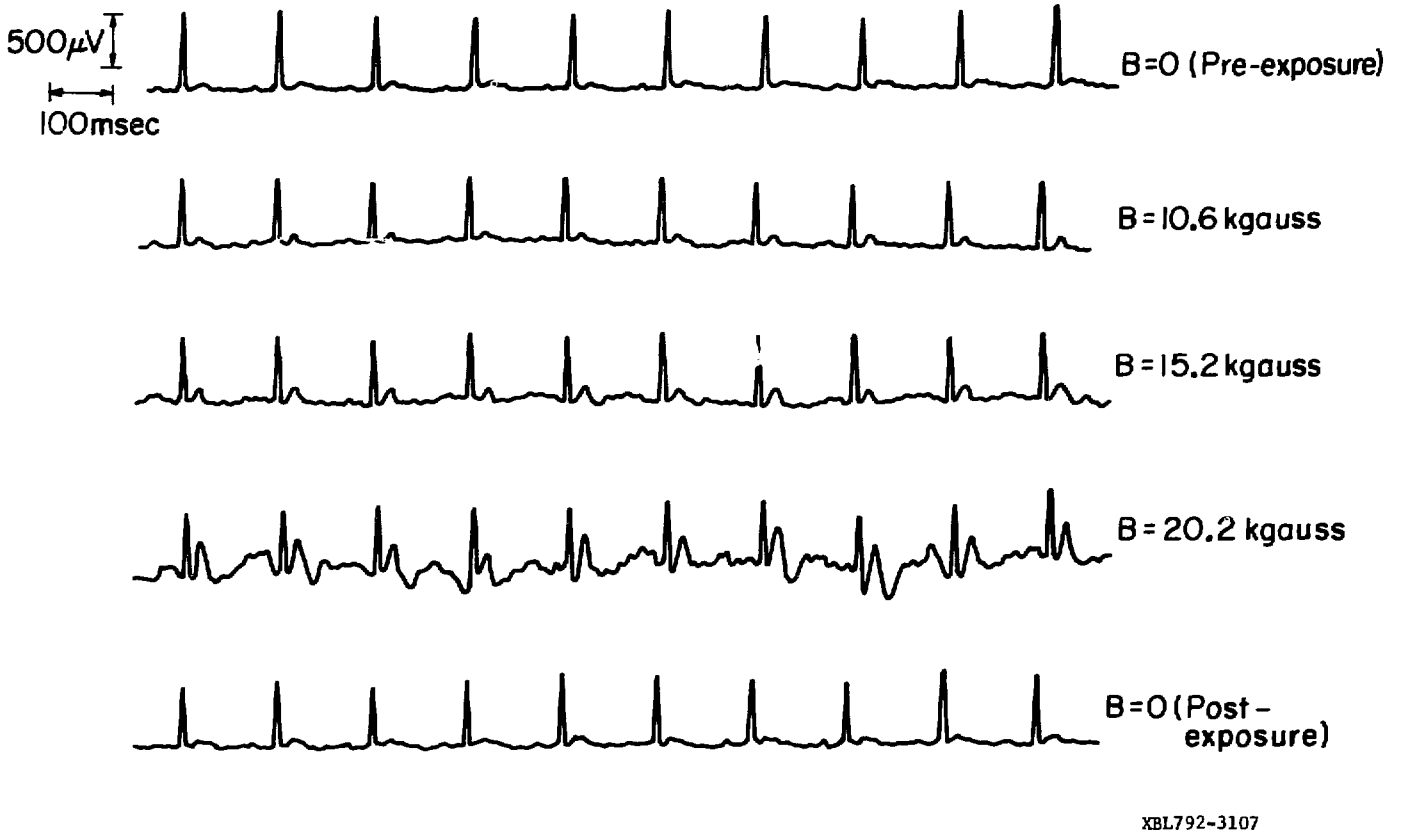
ADULT ♀ BUFFALO RAT ELECTROCARDIOGRAM
500μV
100msec
B=0 (Pre-exposure)
B=10.6 kgauss
B=15.2 kgauss
B=20.2 kgauss
B=0 (Post-exposure)
XBL792-3107

FIGURE 21

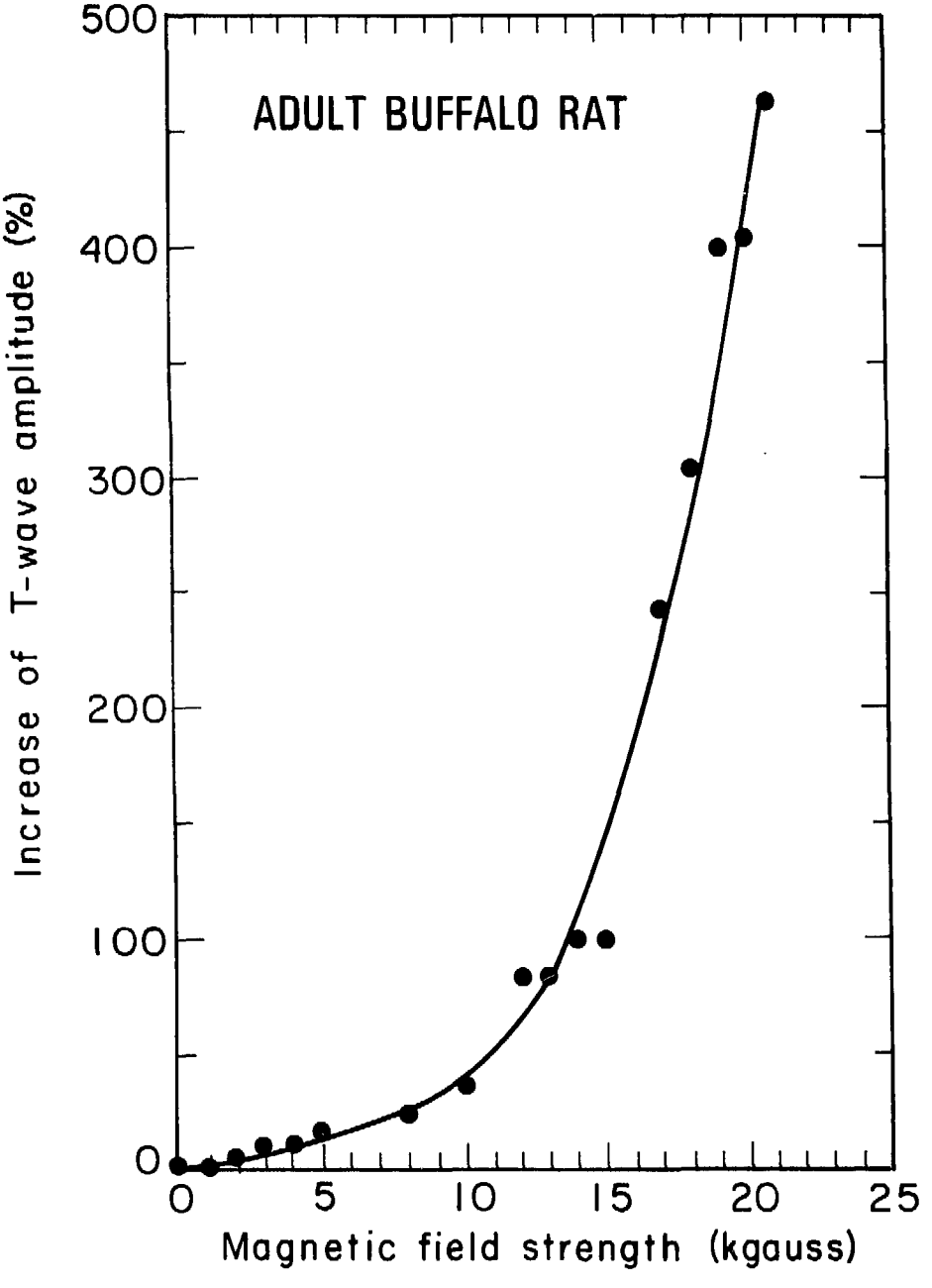
ADULT BUFFALO RAT
Increase of T-wave amplitude (%)
500
400
300
200
100
0
0
5
10
15
20
25
Magnetic field strength (kgauss)
XBL 7810-11557

FIGURE 22

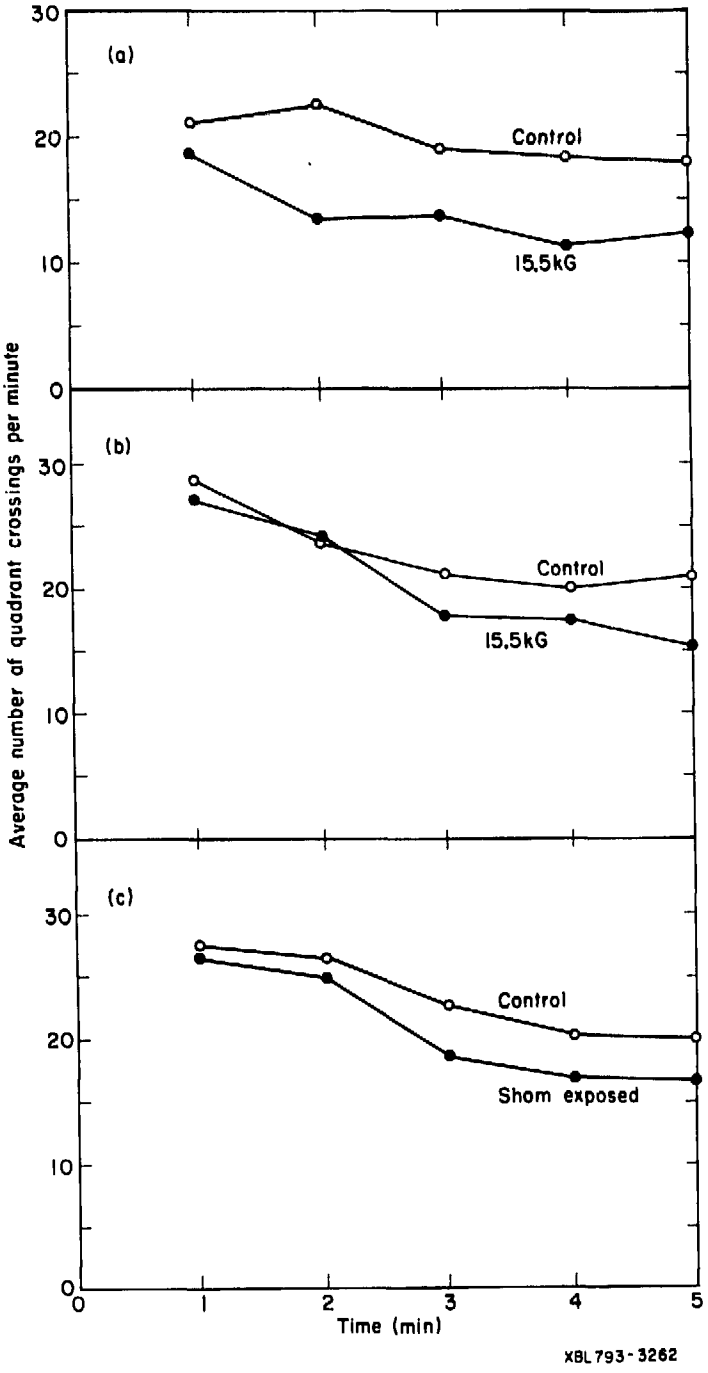
(a)
Control
15.5kG
(b)
Control
15.5kG
(c)
Control
Shom exposed
Average number of quadrant crossings per minute
Time (min)
0
10
20
30
1
2
3
4
5
XBL793-3262

FIGURE 23

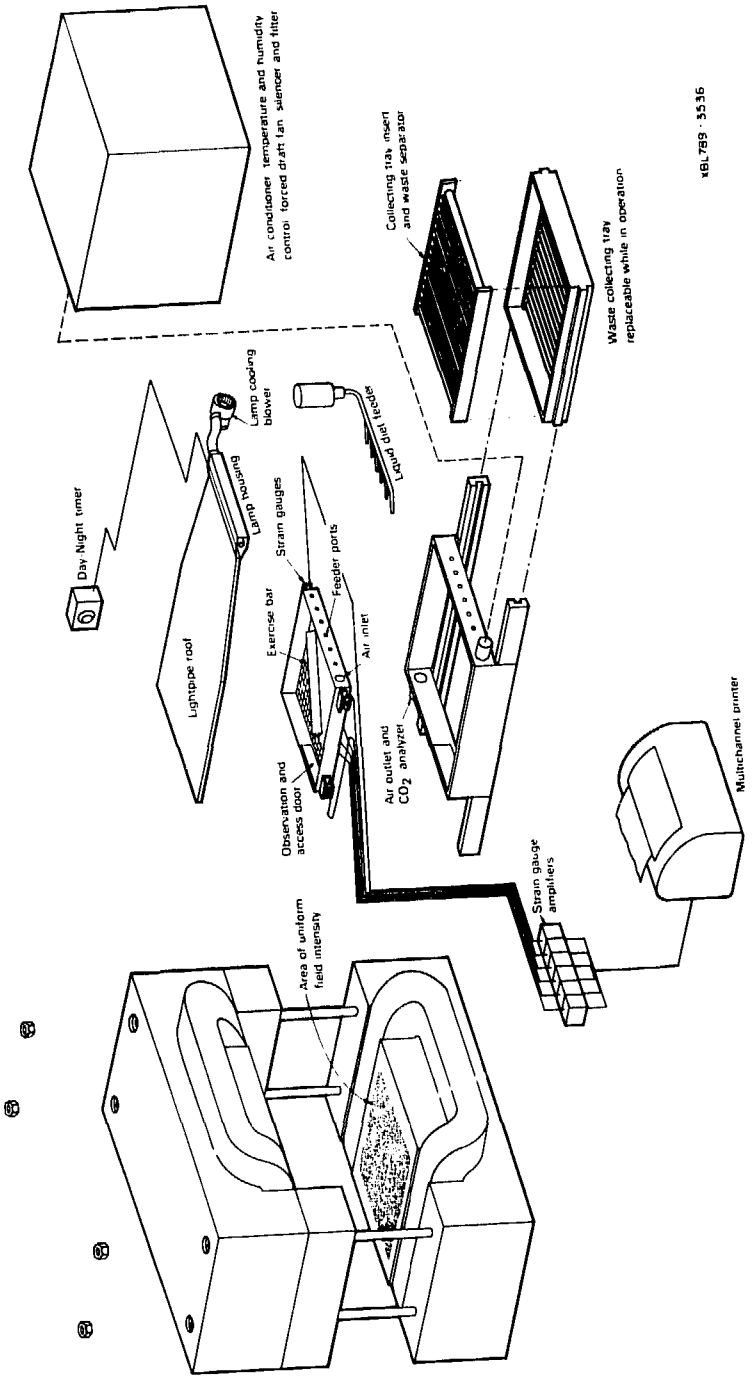
Air conditioner temperature and humidity control forced draft fan silencer and filter
Collecting tray insert and waste separator
Waste collecting tray replaceable while in operation
XBL 789 - 3536
Lamp cooling blower
Lamp housing
Liquid diet feeder
Day Night timer
Strain gauges
Feeder ports
Lightpipe roof
Exercise bar
Air inlet
Observation and access door
Air outlet and CO_2 analyzer
Multichannel printer
Strain gauge amplifiers
Area of uniform field intensity

FIGURE 24

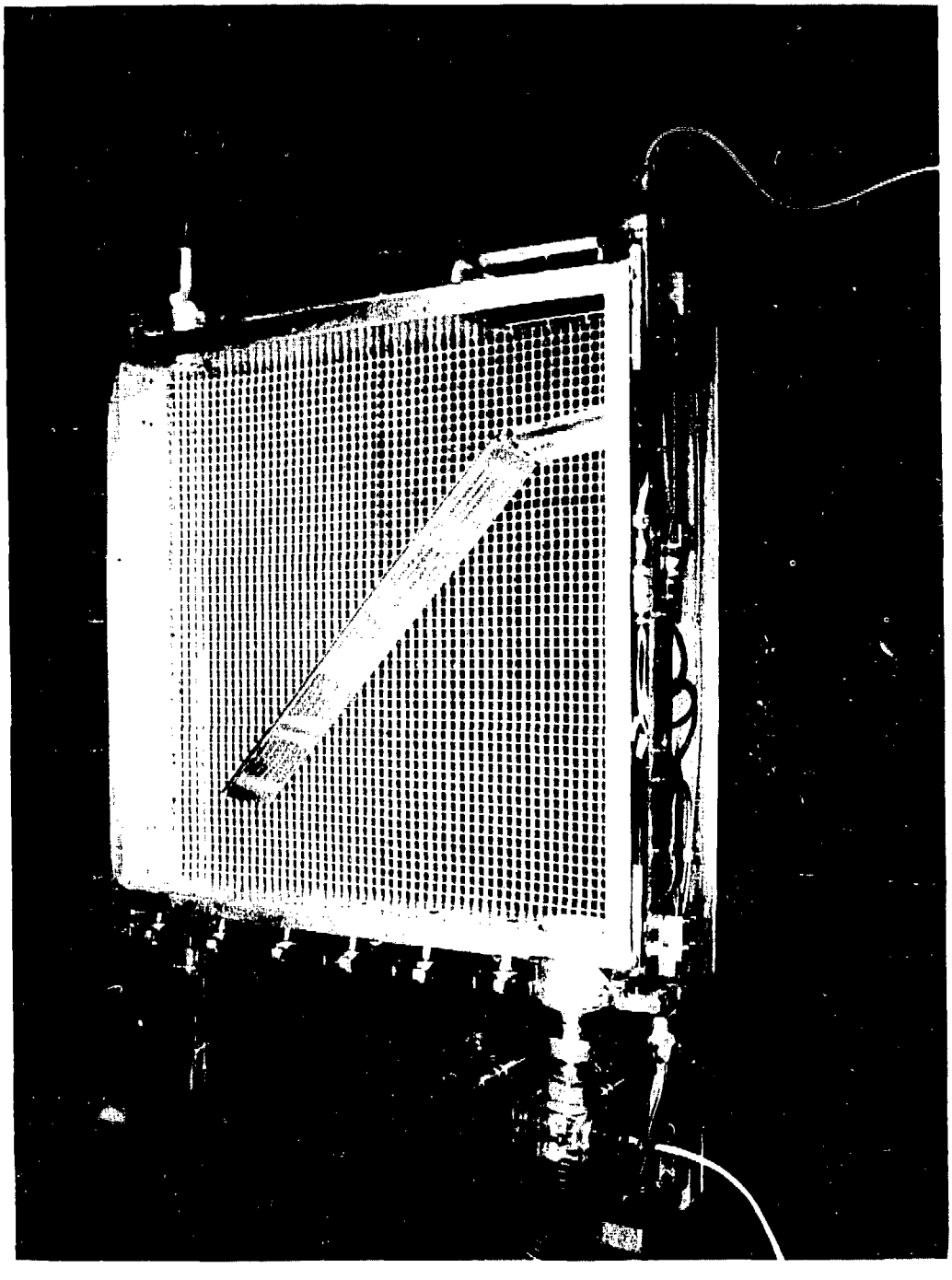

CBB 790-2709

FIGURE 25

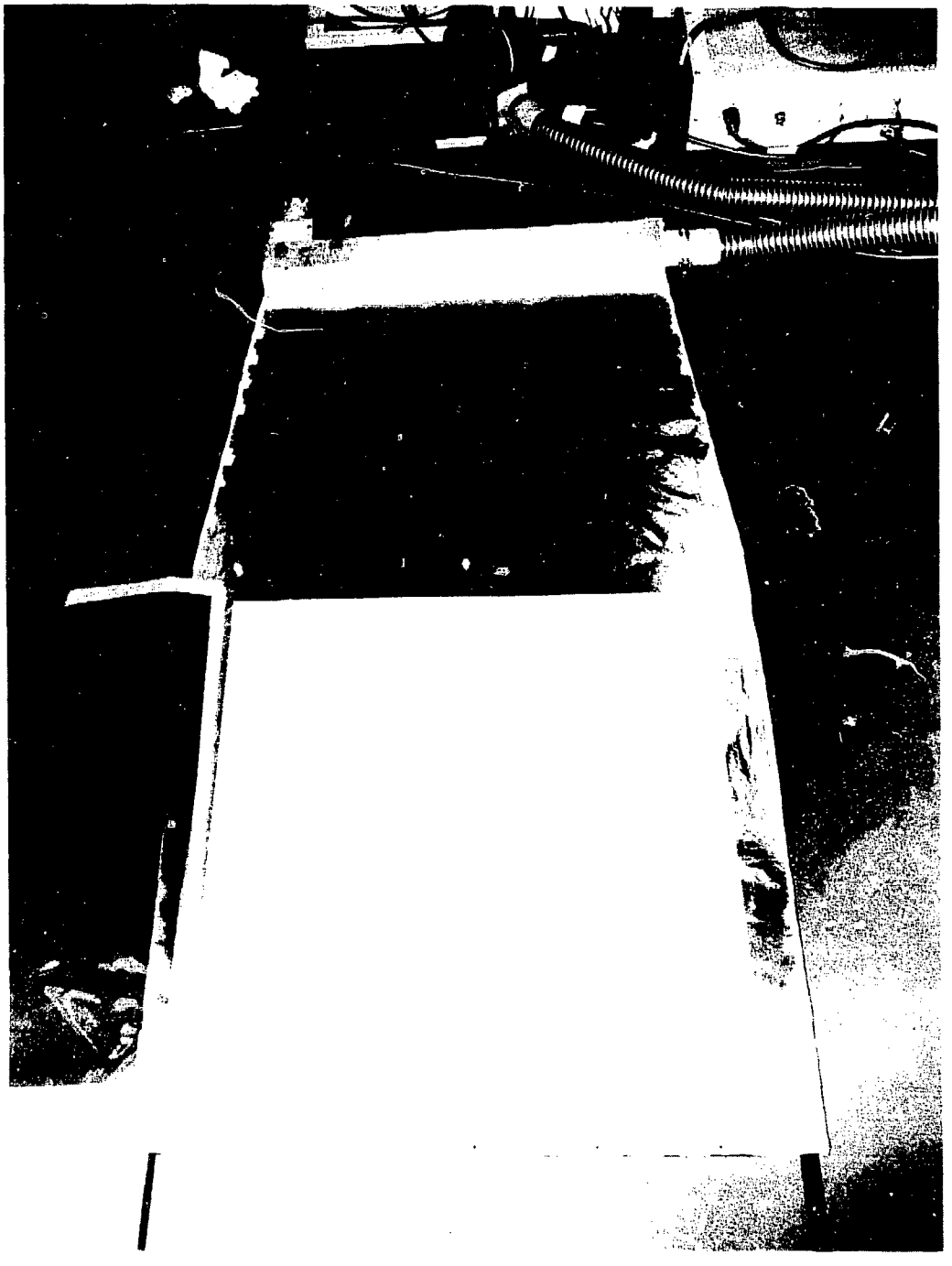

FIGURE 26 CBB 792-2378

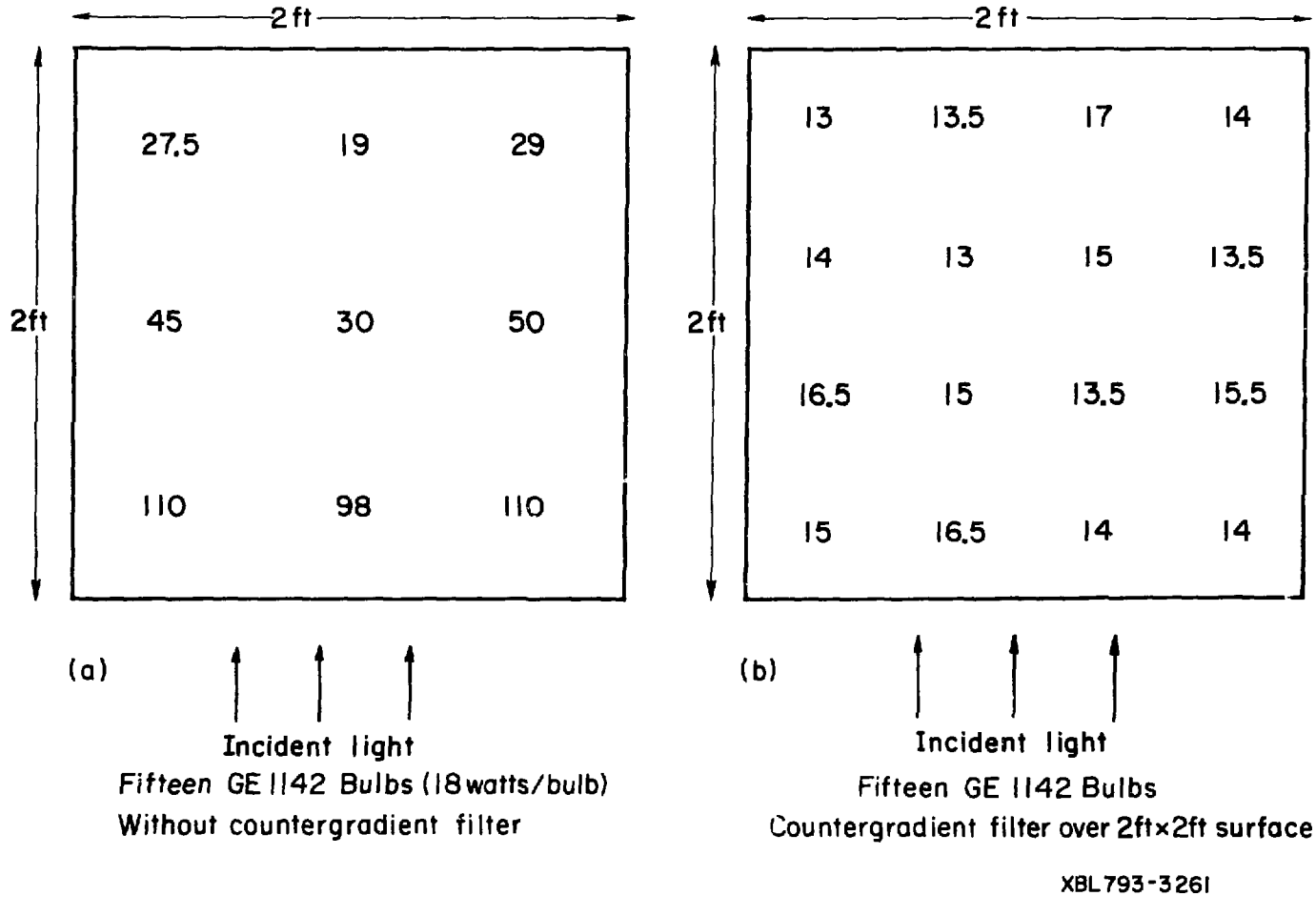
2ft
2ft
27.5
19
29
45
30
50
110
98
110
(a)
Incident light
Fifteen GE 1142 Bulbs (18watts/bulb)
Without countergradient filter
2ft
2ft
13
13.5
17
14
14
13
15
13.5
16.5
15
13.5
15.5
15
16.5
14
14
(b)
Incident light
Fifteen GE 1142 Bulbs
Countergradient filter over 2ft×2ft surface
XBL793-3261

FIGURE 27

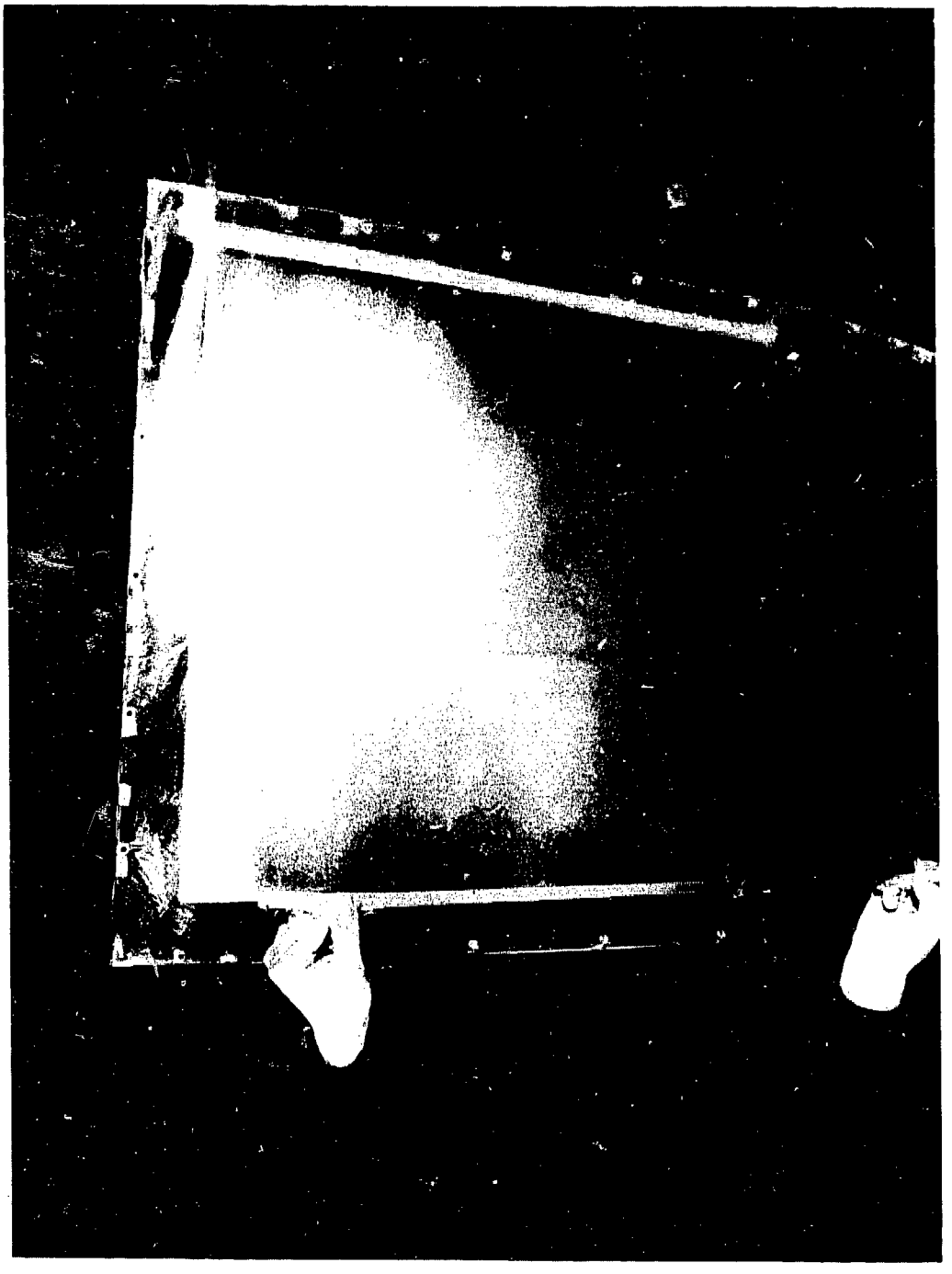

FIGURE 28 CBB 790-2406

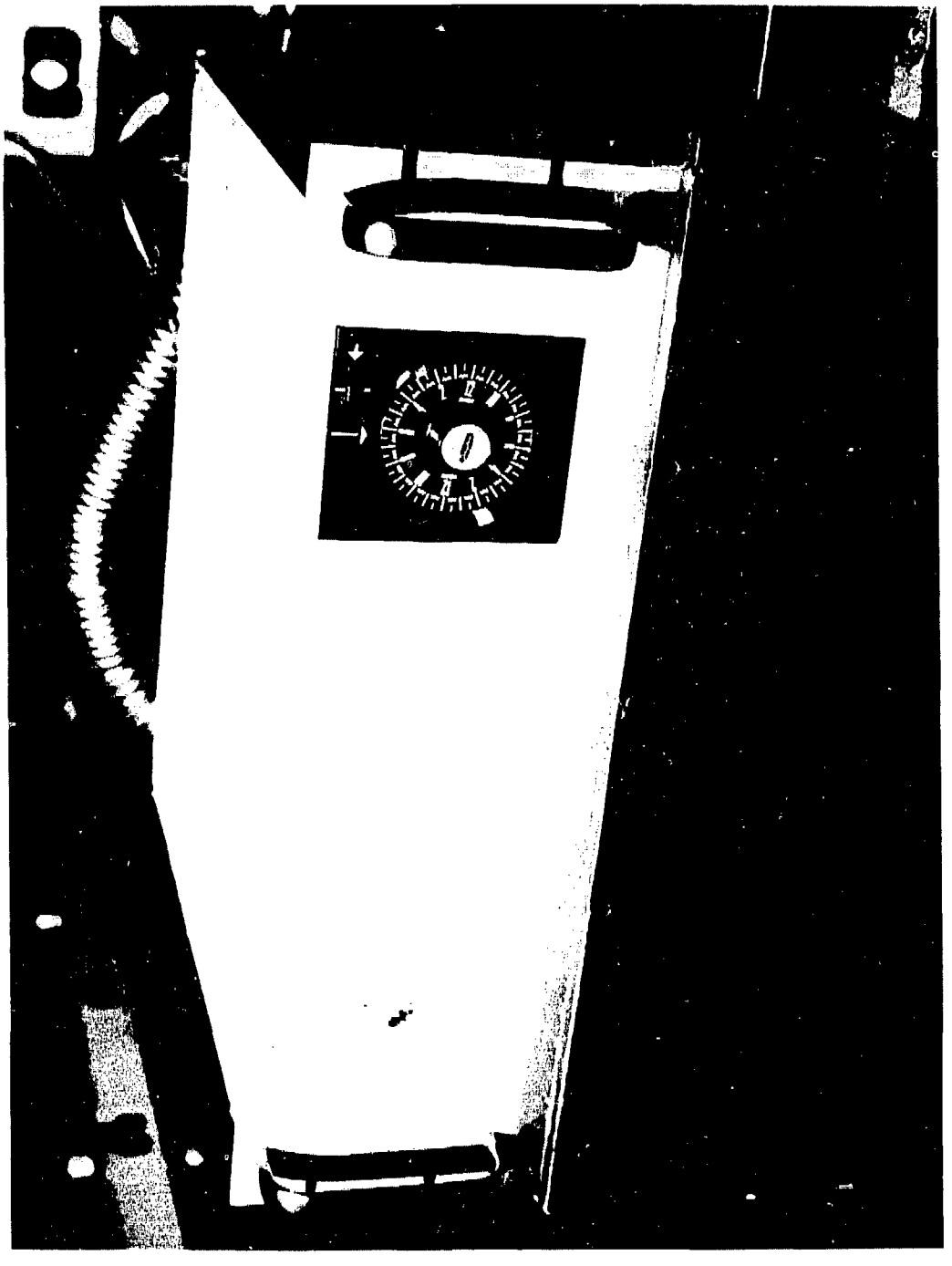

FIGURE 29

CBB 792-2382

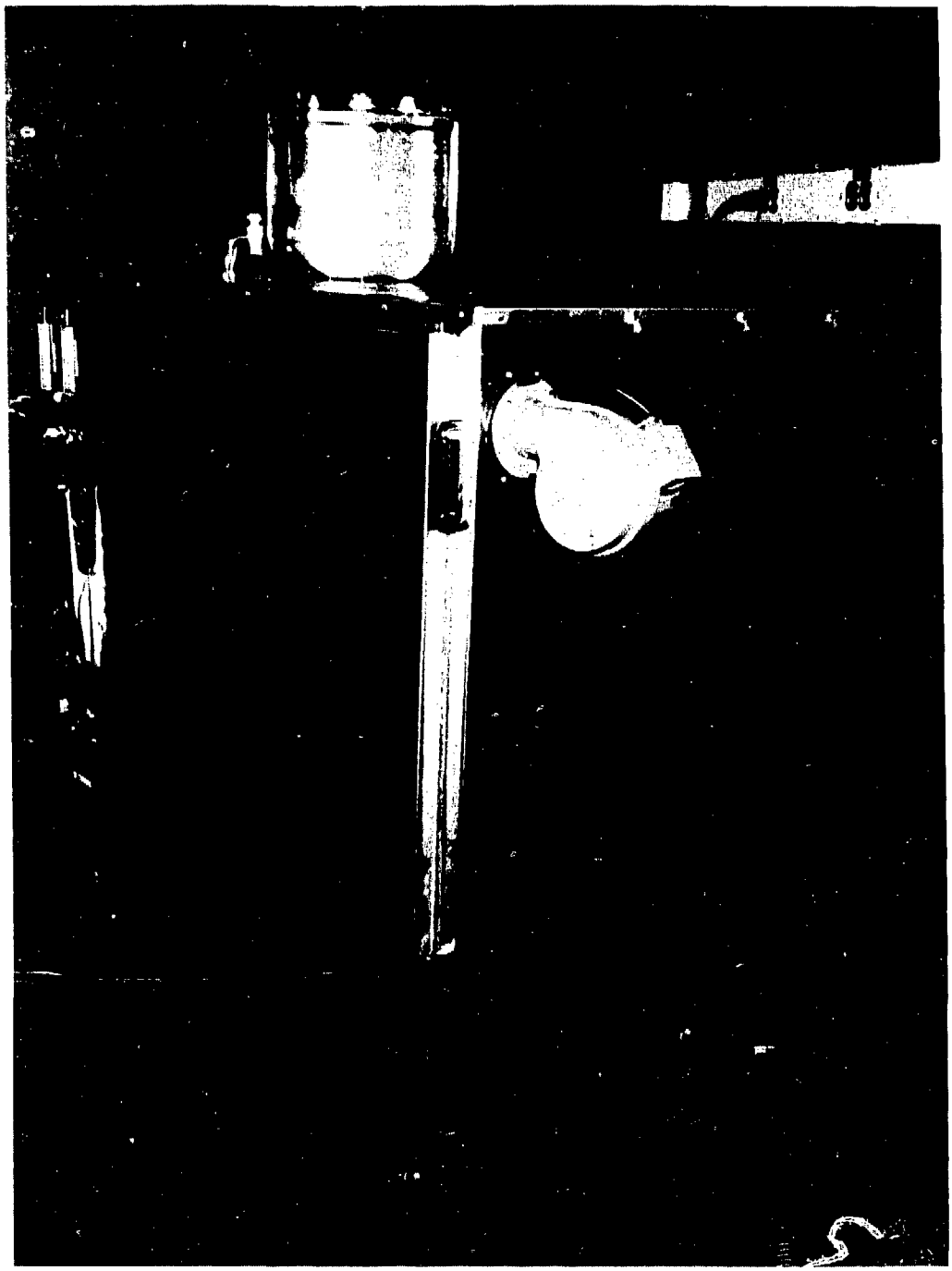

FIGURE 30

CBB 790-2398

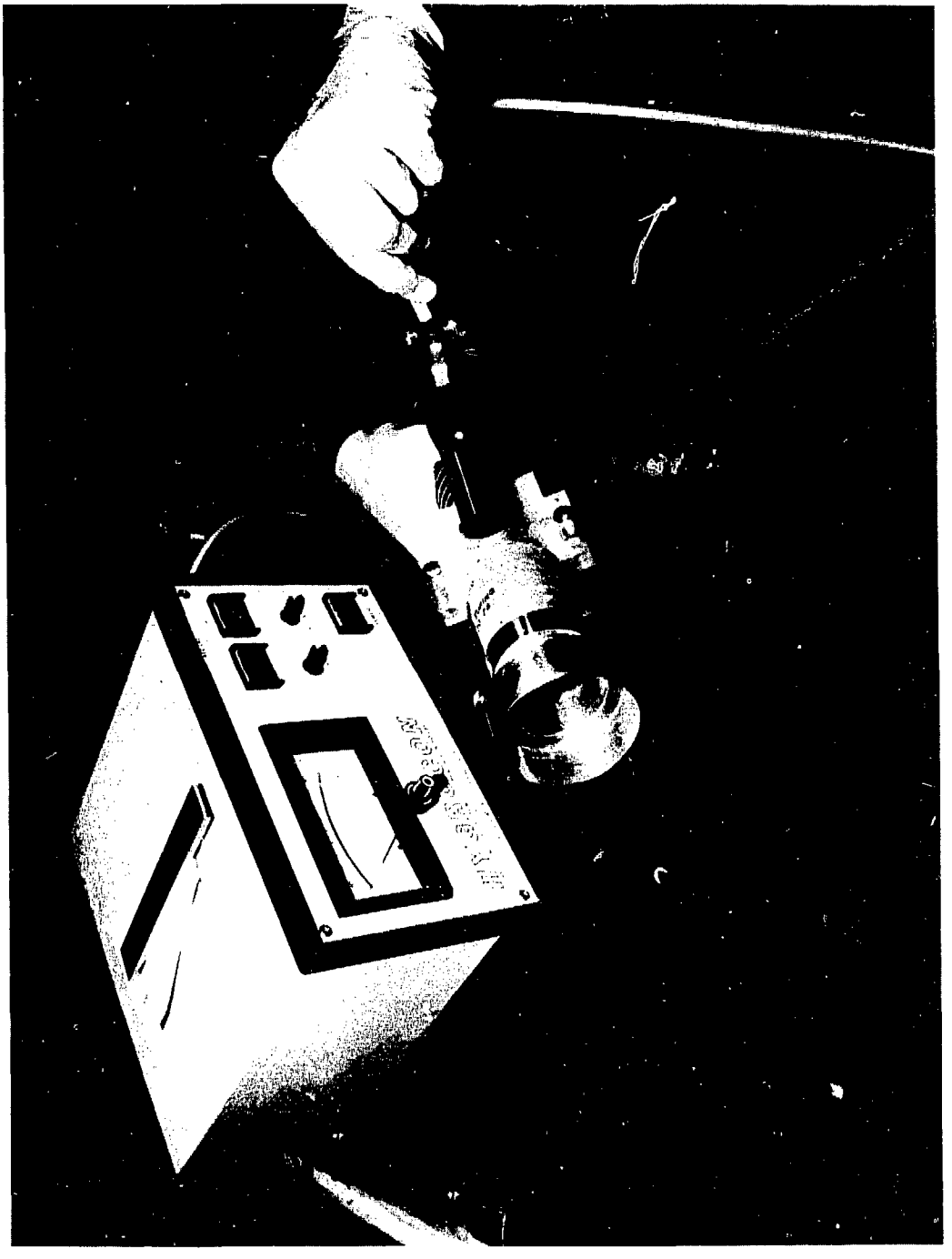

CBB 792-2424

FIGURE 31

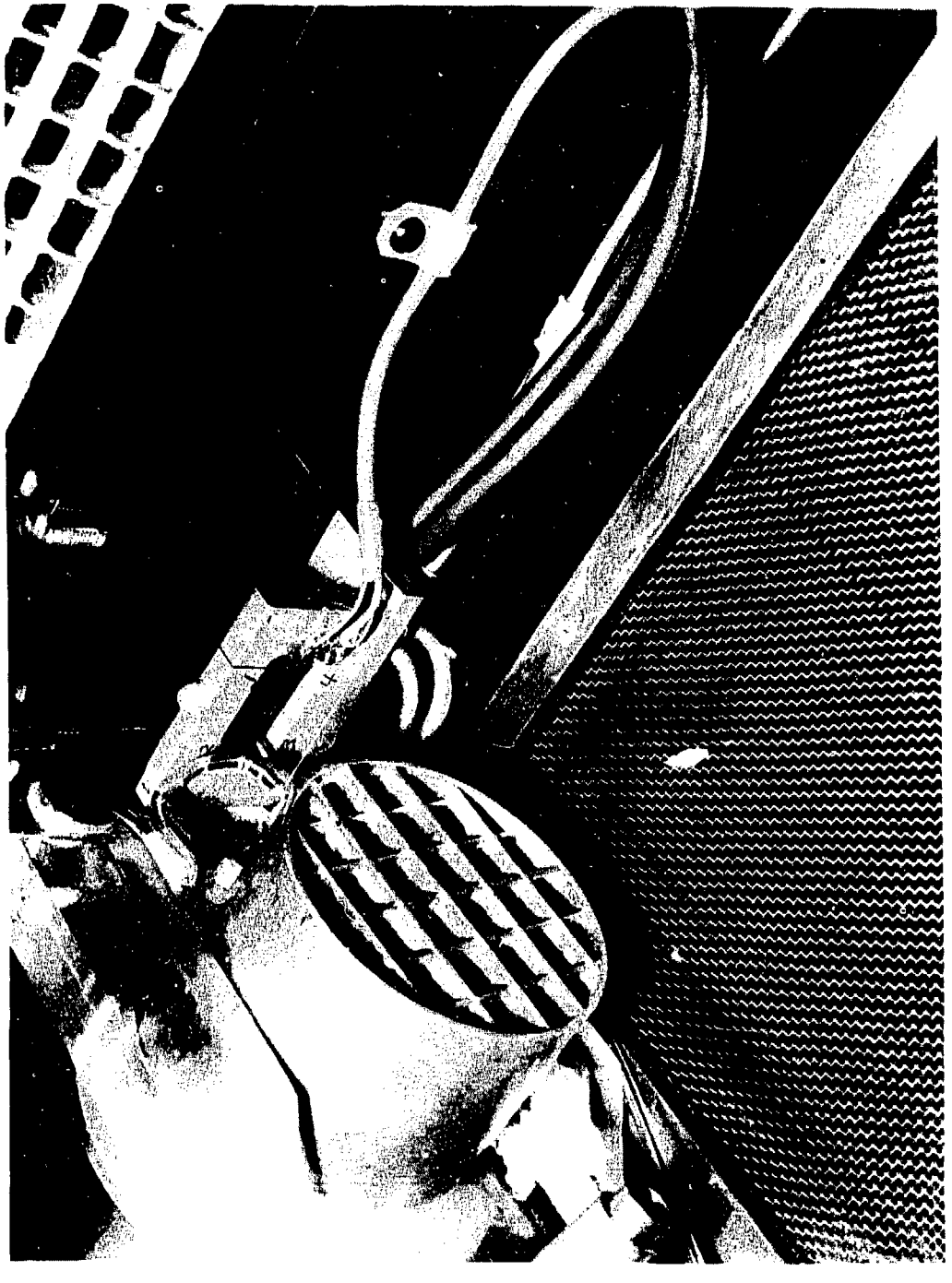

FIGURE 32

CBB 790-2414

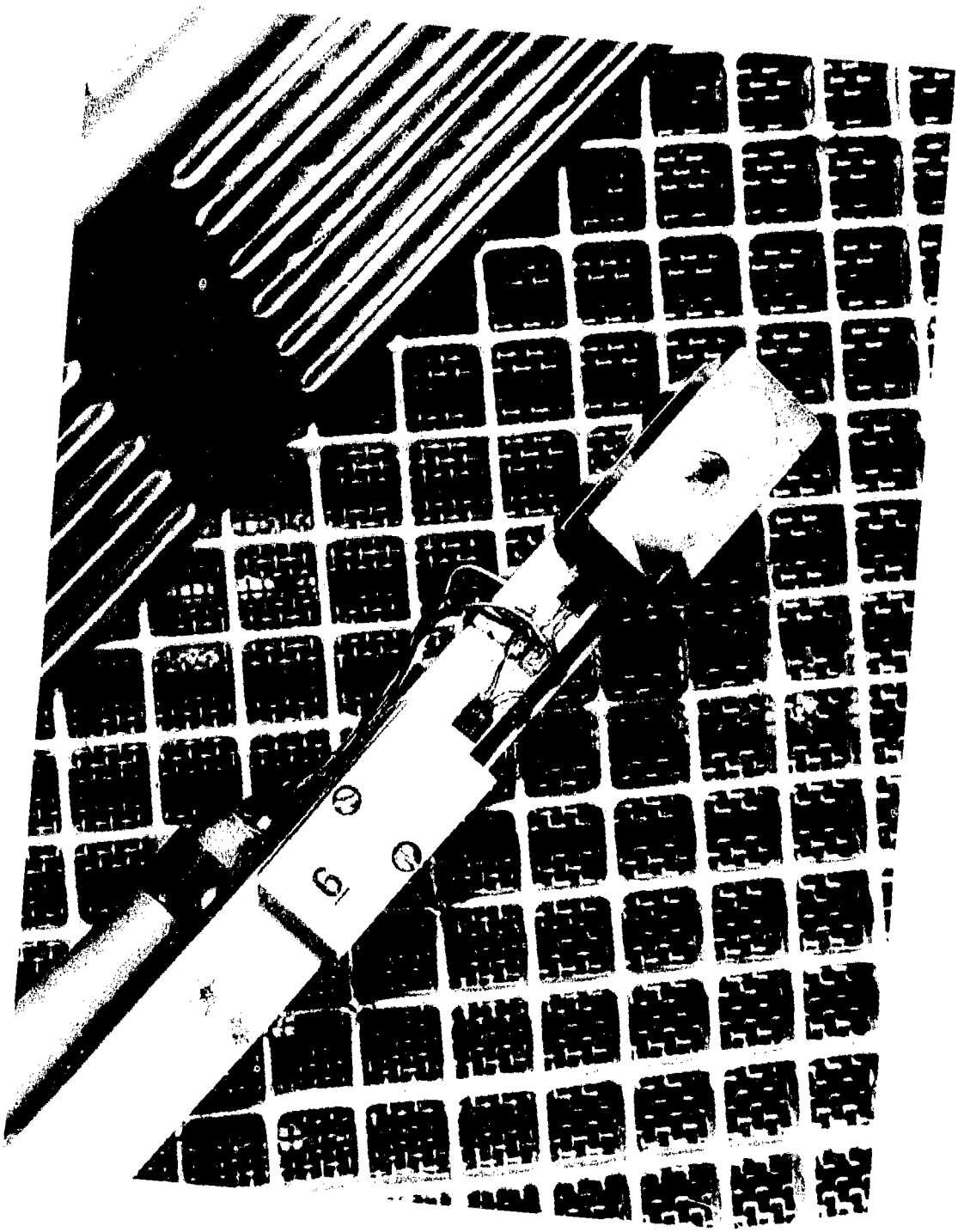

FIGURE 33

CBB 790-2410

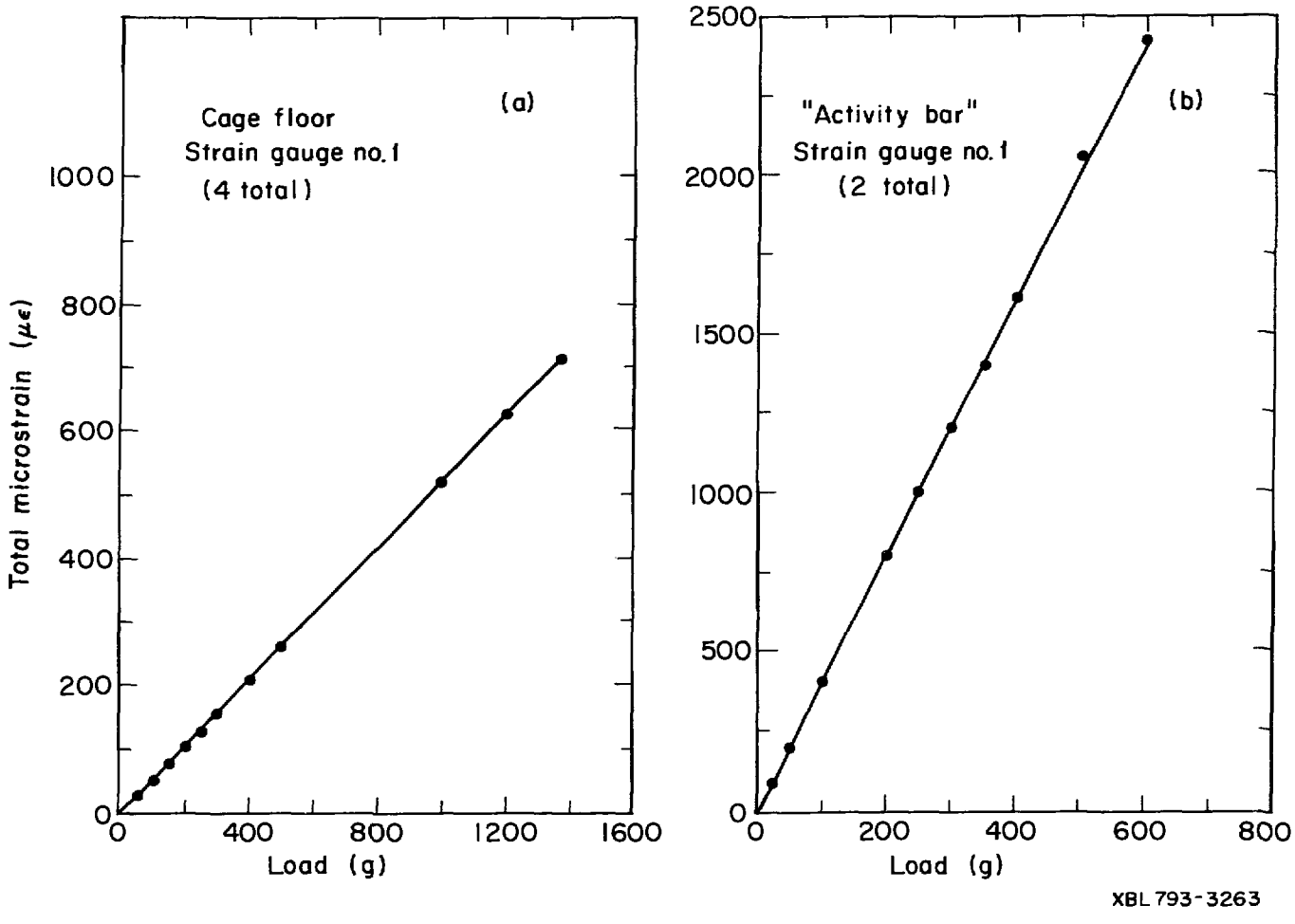
Cage floor
Strain gauge no. 1
(4 total)
(a)
Total microstrain (με)
0
200
400
600
800
1000
0
400
800
1200
1600
Load (g)
"Activity bar"
Strain gauge no. 1
(2 total)
(b)
0
500
1000
1500
2000
2500
0
200
400
600
800
Load (g)
XBL 793-3263

FIGURE 34

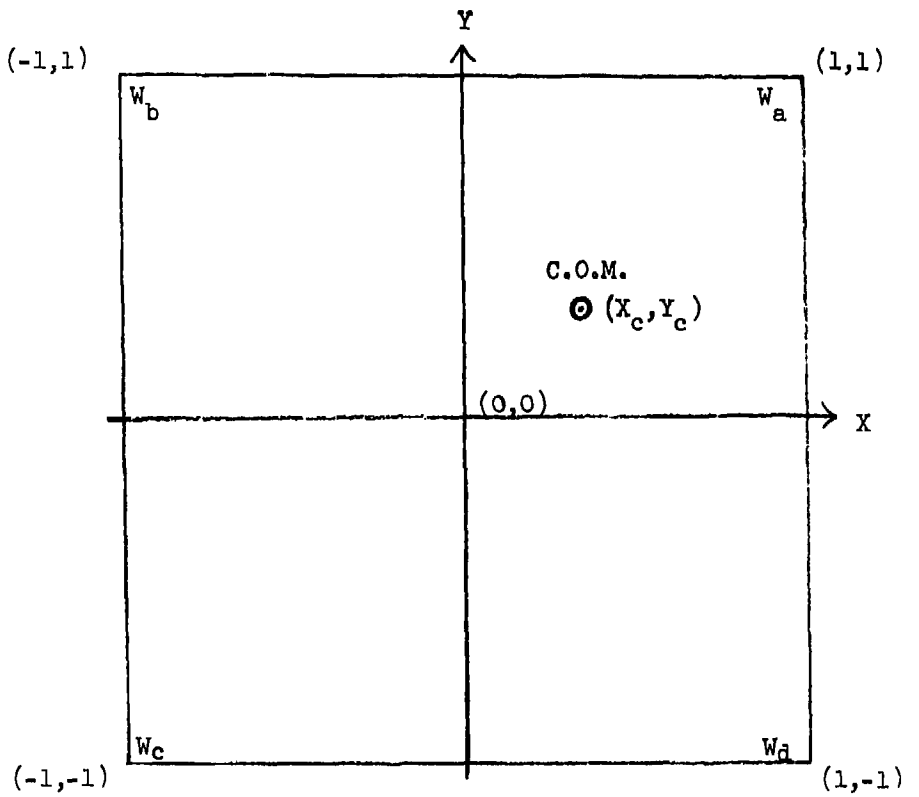

$$W_{total} = W_a + W_b + W_c + W_d$$

$$X_c = \left[\frac{(W_a - W_c) - (W_b - W_d)}{W_{total}} \right]$$

$$Y_c = \left[\frac{(W_a - W_c) + (W_b - W_d)}{W_{total}} \right]$$

XBL 793-8791

FIGURE 35

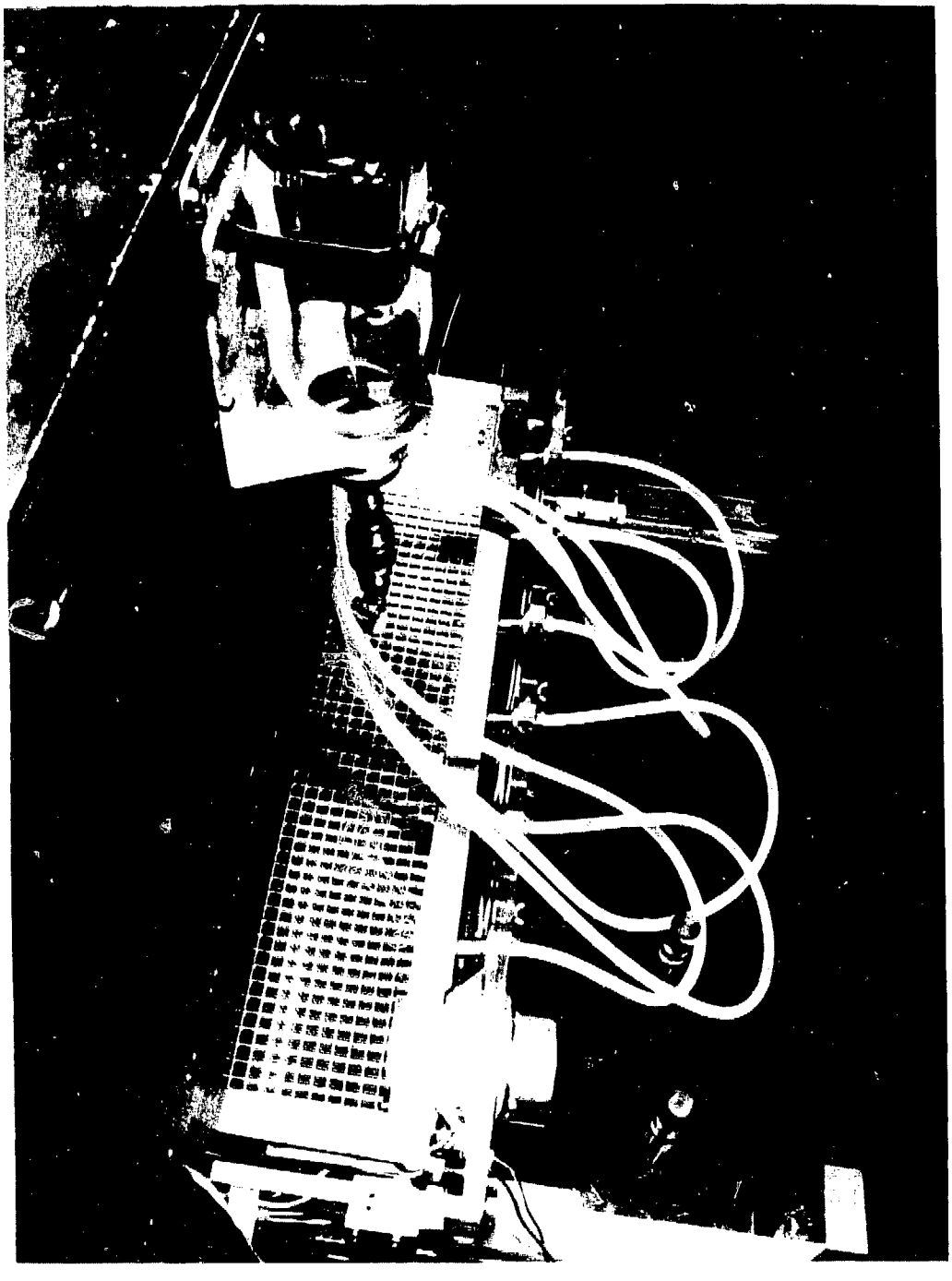

FIGURE 36 CBB 790-2402

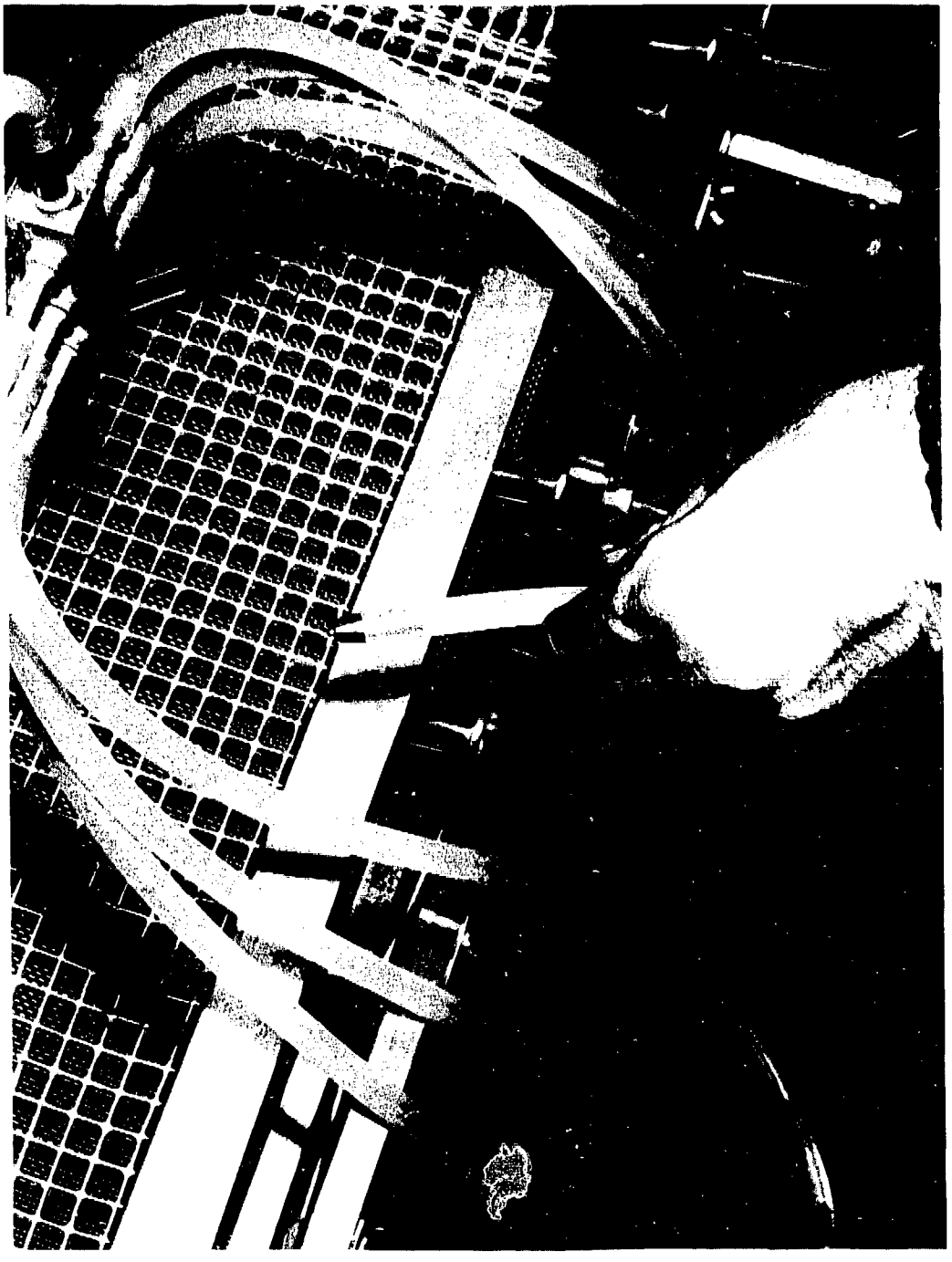

FIGURE 37 CBB 792-2380

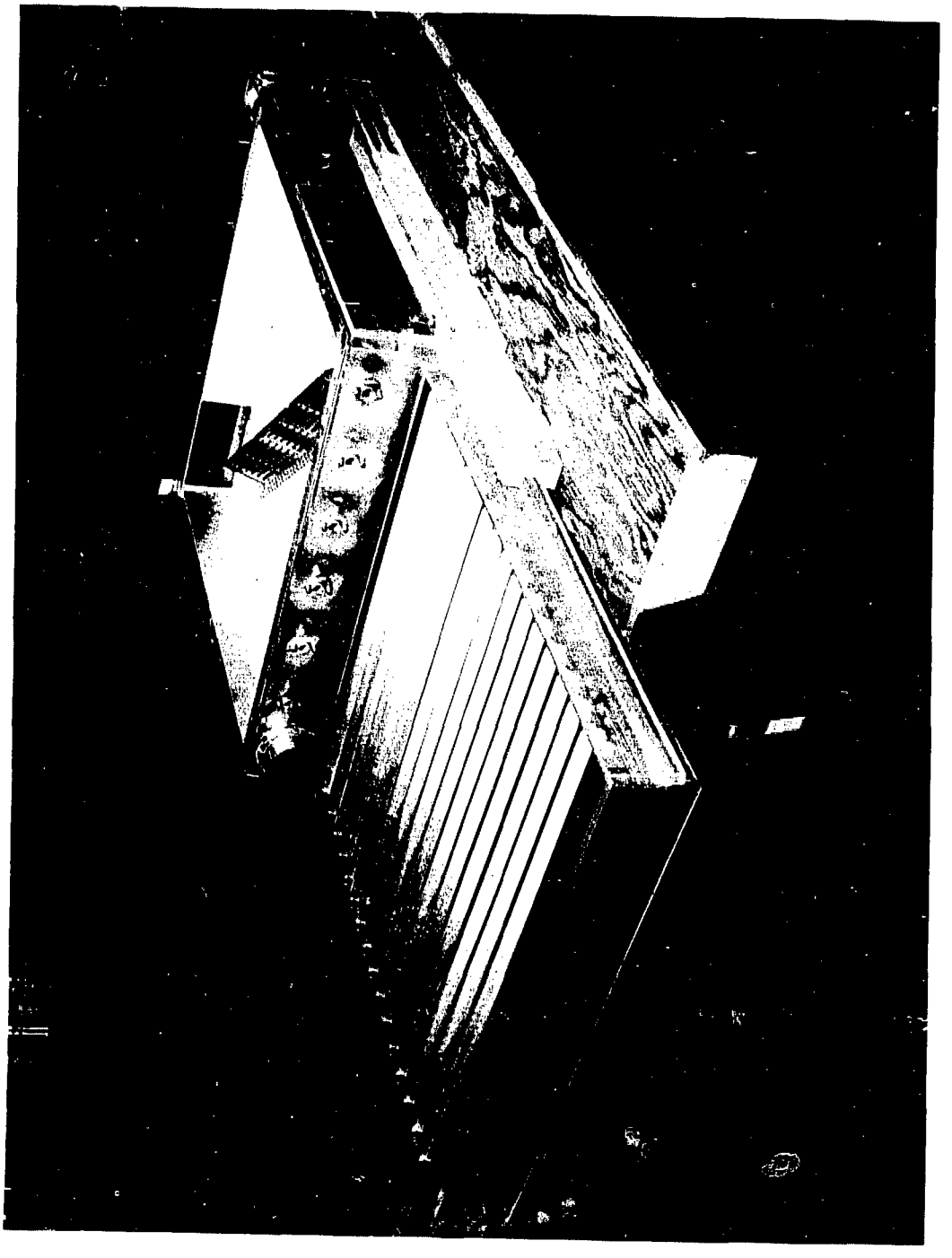

FIGURE 38

XBB 781-1027

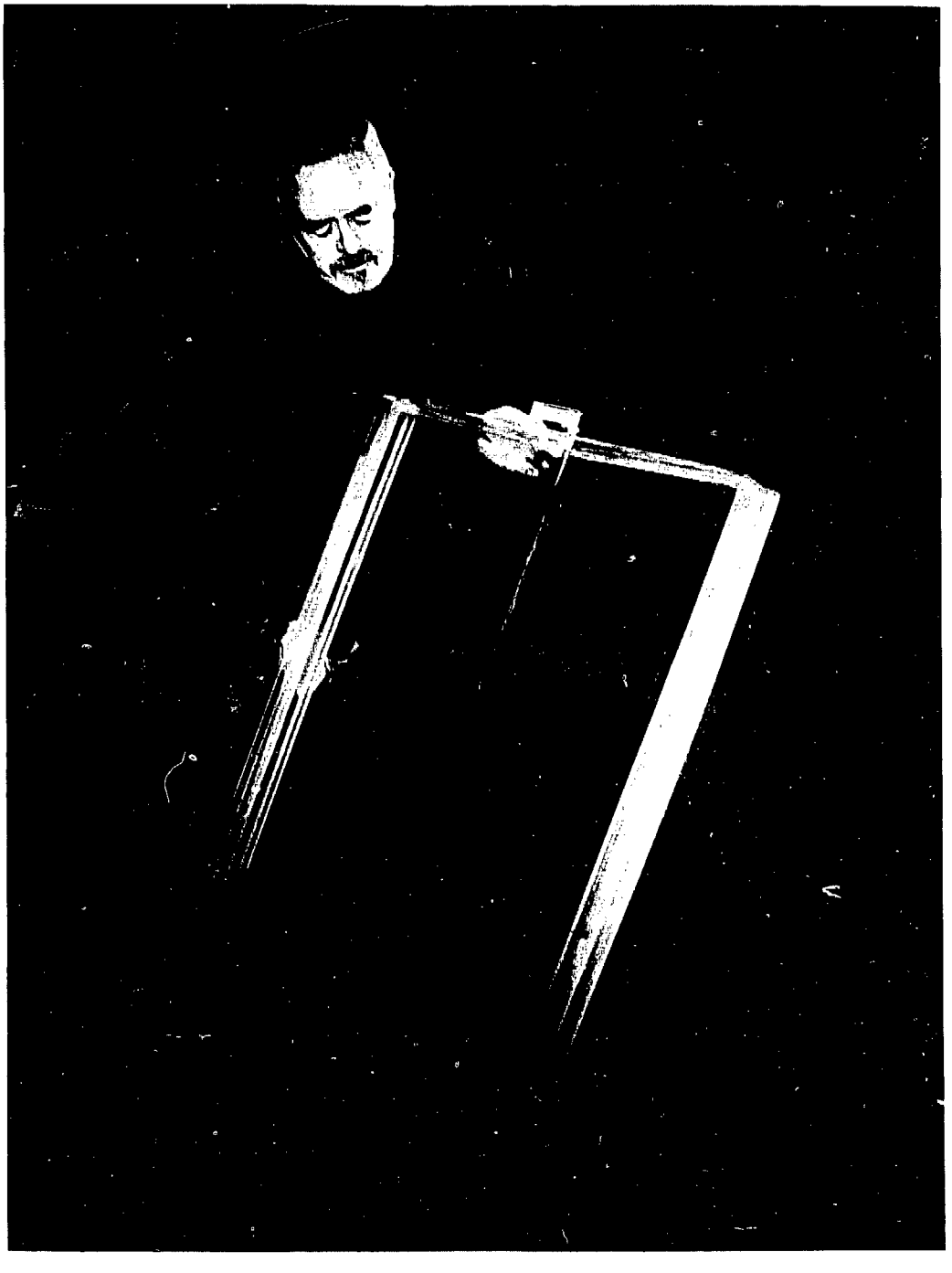

FIGURE 39 CBB 792-2392

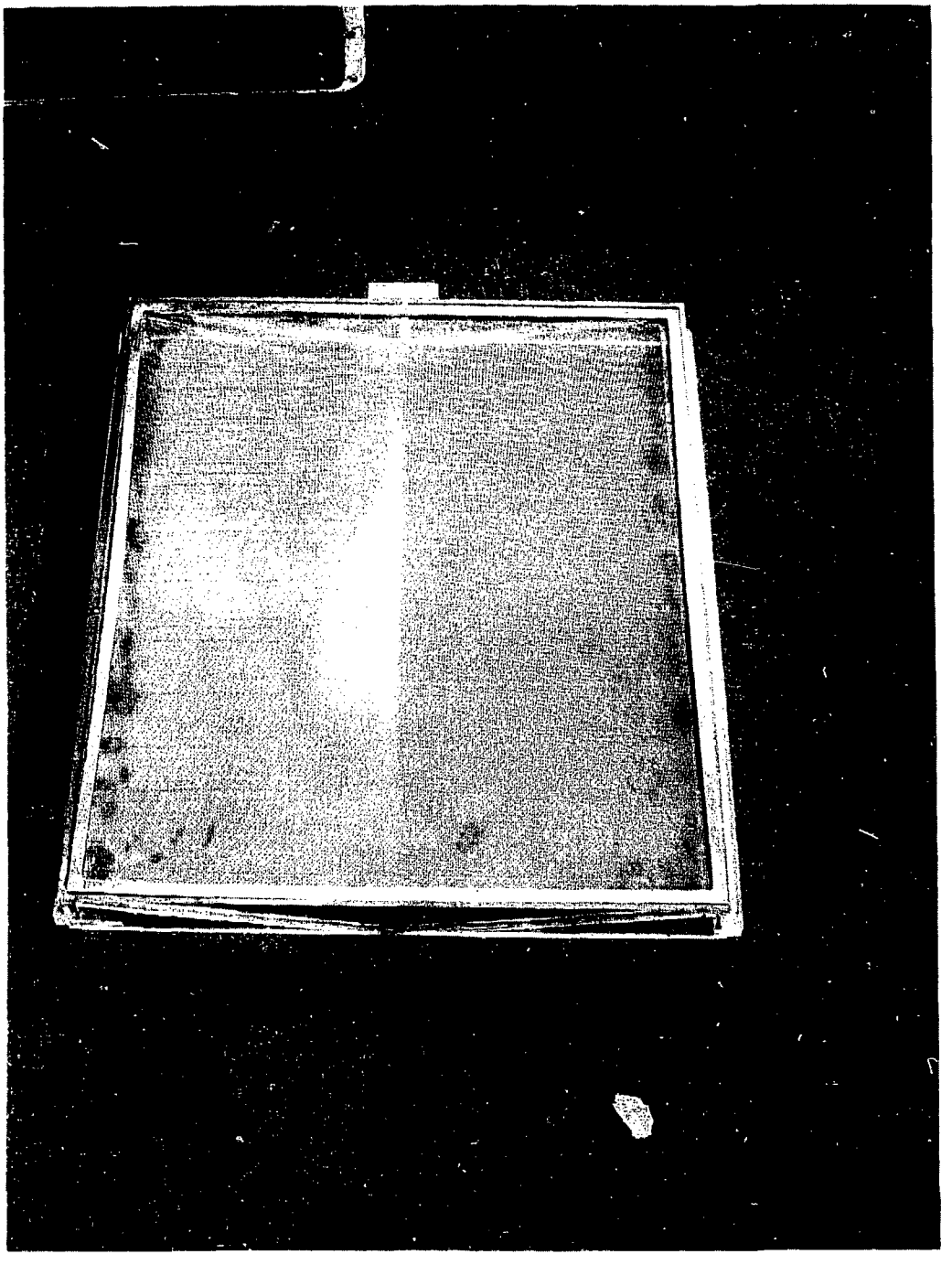

FIGURE 40 CBB 792-2390

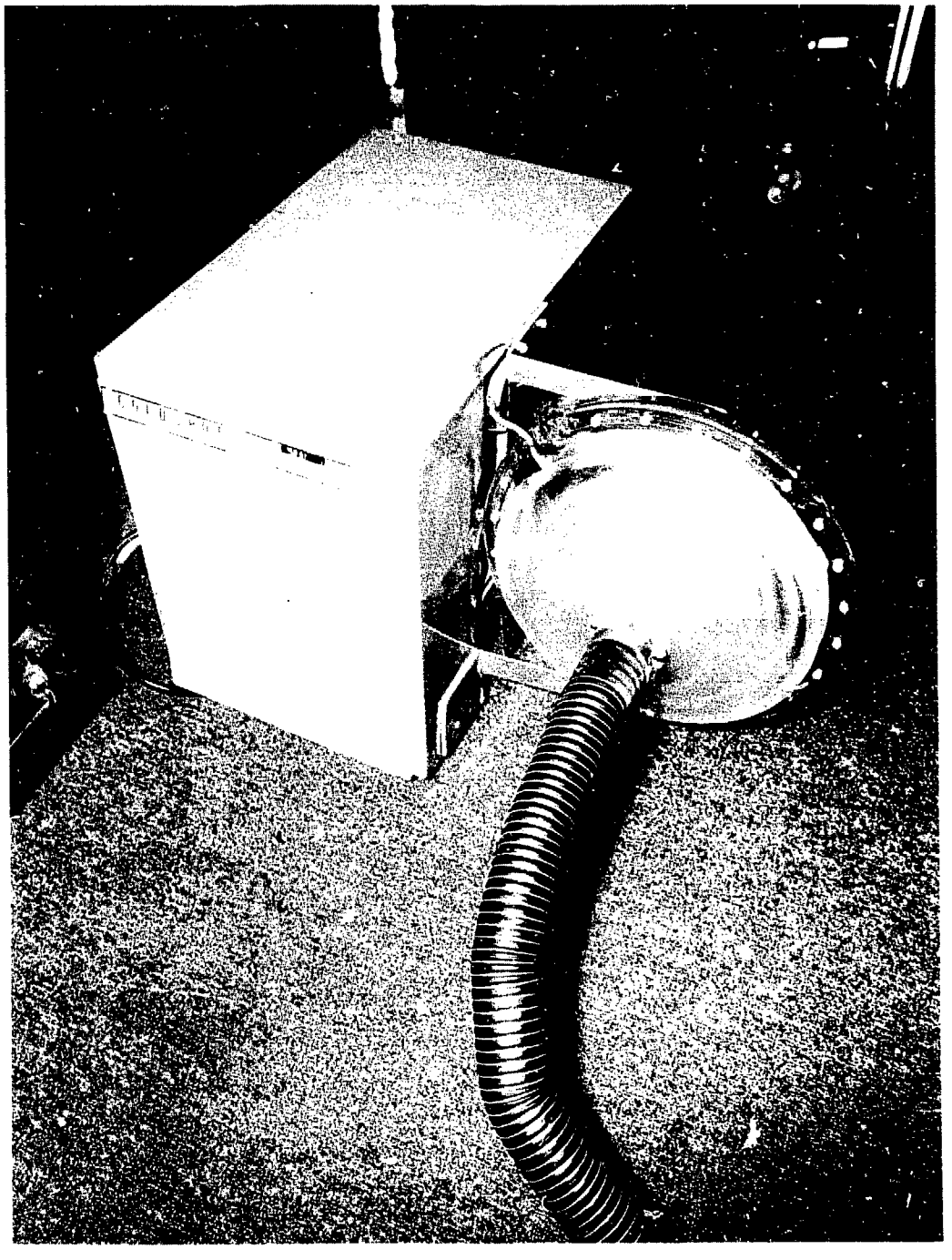

FIGURE 41

CBB 792-2394

FIGURE 42

CBB 792-2386

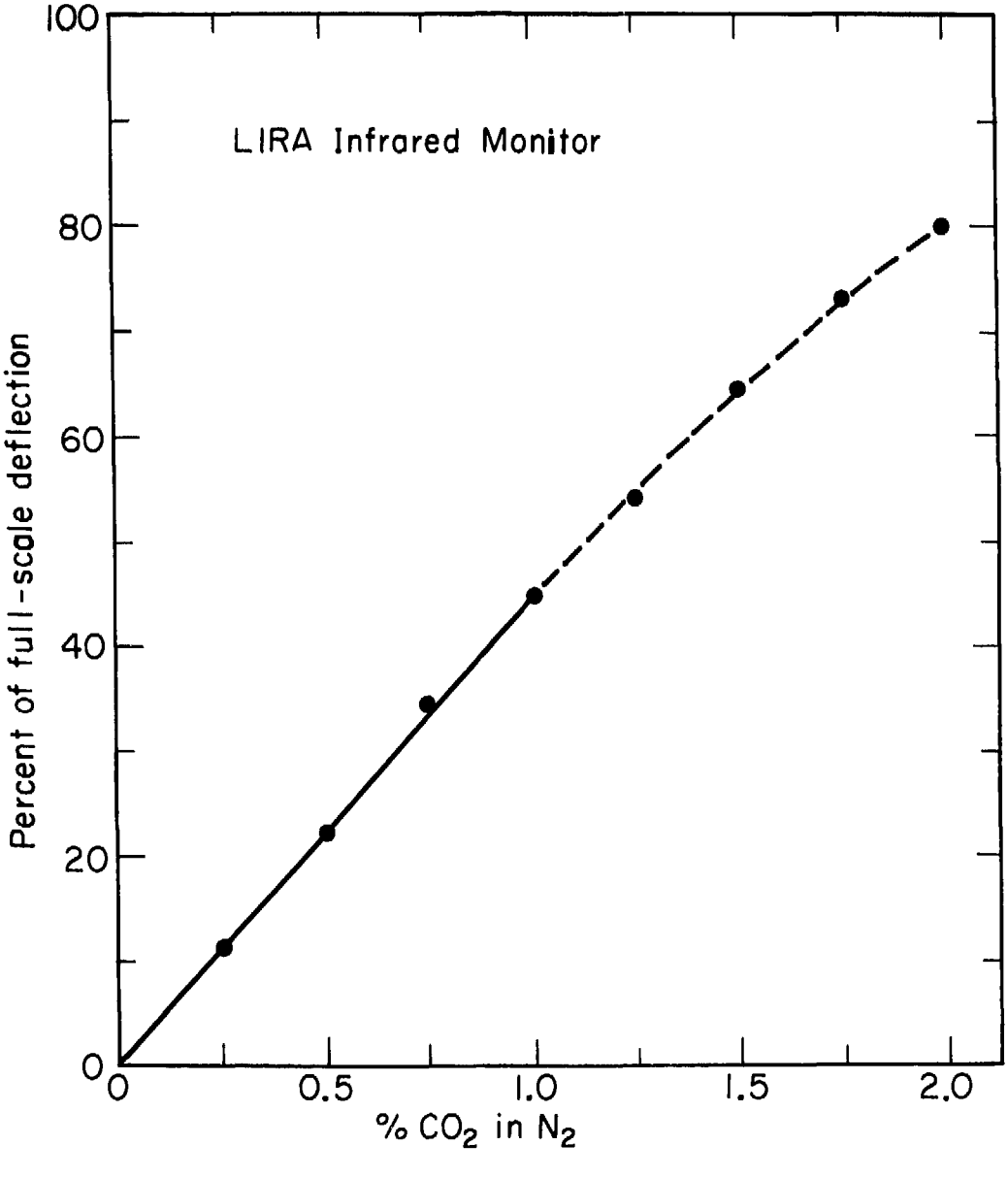
LIRA Infrared Monitor
Percent of full-scale deflection
100
80
60
40
20
0
0
0.5
1.0
1.5
2.0
% CO_2 in N_2
XBL793-3259

FIGURE 43